CLM-R239

CLM-R239

UKAEA

Report

HIGH DENSITY OPERATION IN DITE WITH NEUTRAL BEAM INJECTION

J. Hugill
P.J. Lomas
A.J. Wootton
K.B. Axon
J.E. Bradley
W.H.M. Clark
J.G. Cordey
S.J. Fielding
R.D. Gill
P.C. Johnson
G.M. McCracken
J.W.M. Paul
B.A. Powell
G. Proudfoot
D.F.H. Start

CULHAM LABORATORY
Abingdon Oxfordshire

1983

C/18

Available from H. M. Stationery Office

£3.00

HIGH DENSITY OPERATION IN DITE WITH NEUTRAL BEAM INJECTION

J. Hugill, P.J. Lomas, A.J. Wootton, K.B. Axon, J.E. Bradley, W.H.M. Clark, J.G. Cordey, S.J. Fielding, R.D. Gill, P.C. Johnson, G.M. McCracken, J.W.M. Paul, B.A. Powell, G. Proudfoot, D.F.H. Start

Culham Laboratory, Abingdon, Oxon, OX14 3DB, UK
(Euratom/UKAEA Fusion Association)

ABSTRACT

The highest density discharges are produced by simultaneous neutral beam injection at $P_{inj} \lesssim 1$MW and cold gas feed. Energy balances show electron and ion heat conduction are the most important losses from the discharge centre. Ion conduction is increasingly important as the density is raised and is $\sim$ 1-4 times neoclassical expectation. The measured changes in conduction coefficients on injection do not suggest any marked deterioration of confinement. However, global measurements of β and τ_E over a wide range of discharge parameters show the energy content increases only slowly with P_{inj} and density and strongly with plasma current. These results can be interpreted as a soft limit on β_p at $\beta_p \approx 1$ or an unfavourable scaling of confinement with temperature. Ideal high-n ballooning modes are theoretically stable at the β-values reached. The empirical scaling obtained also fits a range of results from other devices, including those with ohmic heating. The density clamp which occurs with injection in some cases, is overcome by increasing the gas feed rate. Measurements in the scrape-off plasma show that it is associated with an increase in energy and particle fluxes to the limiters, consistent with the decrease in particle containment time. The density is limited by disruption preceded by fast-growing m = 2 modes. Injection produces no substantial increase in the maximum density, $\bar{n}_e(\max)$ attained for $q \gtrsim 4$, even when the power input exceeds the ohmic power by an order of magnitude. This suggests that the intermediate cause of disruption is not excessive radiation from the periphery. For $2<q<3$, $\bar{n}_e(\max)$ is increased up to 2.5 times by a modest amount of neutral beam power. Thereafter a new limit is reached which appears to be an extension of the high-q limit. It is proportional to mean current density and insensitive to P_{inj}.

March 1983

ISBN 0 83511 122 7

1. INTRODUCTION

This paper describes experiments on DITE [1] tokamak to determine the maximum density which could be achieved with ohmic heating and with the injection of up to 1MW of fast neutrals. Energy balances are constructed for some typical high density discharges, and the behaviour of global confinement and β-values at high density is discussed. For some conditions injection produces a density clamp as reported for ISX-B [2]. This phenomenon is discussed in detail and an explanation proposed. The nature of the disruptive density limit with high power neutral injection and the scaling of this limit is investigated in depth. Where not explicitly given, MKS units are implied.

2. METHOD OF OPERATION AND GENERAL DISCHARGE BEHAVIOUR

In the experiments described the working gas is deuterium. The vacuum vessel is usually gettered with titanium [3], though some experiments used only short pulse (20kA, 20ms) discharge cleaning in deuterium and/or glow cleaning (5A DC, 400V) in hydrogen at 10-30mtorr. The limiters consist of two pairs of semi-circular arcs of titanium with minor radius, $a \simeq 0.26$m centred on a major radius, $R = 1.17$m. These are supplemented by two carbon limiters of internal radius 0.25m subtending 80° at the centre of the vacuum vessel and movable vertically. The major radius of the plasma is controlled by a feedback system and can be varied at will. The toroidal field, B_T is varied from 0.9 to 2.7T, the plasma current, I_p from 40 to 260kA and the limiter q-value is $\gtrsim 2$.

The line average plasma density, $\bar{n}_e \lesssim 10^{20}$ m^{-3} is controlled by cold gas feed via programmable piezoelectric valves admitting gas

through a single port. The distance from the gas inlet to the nearest titanium limiter surface is approximately 1.8m.

Two injector lines each with two sources inject H beams with a total power, P_{inj}, $\lesssim$ 1.0MW and 100ms pulse length. Both beams are directed tangentially in the same sense. Usually, coinjection is used. The $H^+ : H_2^+ : H_3^+$ species ratio in the extracted beams is 73 : 15 : 12 with a small percentage of light impurities ($\lesssim$ 3%). The accelerating voltage is typically 22-26kV.

The diagnostics used for these experiments are listed in Table I.

The sequence of operation in a typical run of approximately 50 discharges is as follows:

a) Set up a 200-300ms duration ohmic discharge at the required levels of B_T and I_p.

b) Increase $\bar{n}_e$ by cold gas feed (usually at a constant rate starting at discharge initiation, t = 0) until the density limit is reached at t = 150-200ms.

c) Apply a 100ms neutral beam pulse with P_{inj} = 0.2-1.0MW starting at t $\sim$ 100ms. In certain conditions this produces a density 'clamp' (see Section 5), which is overcome by stepping up the gas feed rate during neutral beam injection.

d) Increase the additional gas feed rate until disruption occurs during the injection pulse.

e) Study the discharge obtained, or vary parameters of interest, such as P_{inj}, I_p, gas feed rate etc., to optimise conditions.

Figure 1 shows the high density limit obtained by these procedures [10] at B_T = 1.35T, using neutral injection. The region of stable operation in $1/q$ v $\bar{n}_e$ R/B_T space with ohmic heating has been extended over that first obtained in DITE [1] (curve A) by gettering [3] and

operation at low-q [11] aided by the change in limiter material from molybdenum to titanium (curve B). With neutral injection, it is possible to extend the region of operation to curve C in Figure 1. For comparison, maximum densities obtained on other tokamak devices [2,12-20] are shown in Figure 2.

Injection invariably produces an increase in β, ion temperature, T_i, and total radiation and a reduction in loop voltage, V_ℓ. For $\bar{n}_e \gtrsim 2.10^{19}$ m^{-3} the central electron temperature, T_{eo} also increases. β continues to rise as $\bar{n}_e$ is increased during neutral injection but T_{eo} and T_{io} fall. The global energy confinement time, τ_E, which is calculated from the plasma diamagnetism and the total power input, increases with $\bar{n}_e$ in the ohmic phase but, during injection, τ_E is smaller and increases less strongly with $\bar{n}_e$. The total radiation is typically 20-30% of the power input in the ohmic phase. During injection the power radiated, as measured away from the neutral beams, increases up to 40% of the total power input, but is no longer axisymmetric [21]. The discharge ends with a series of disruptions if $\bar{n}_e$ is sufficiently high. At lower densities it can remain stable until the current has fallen to $\sim$ 10kA, when position control is lost and there is a terminal disruption.

3. POWER BALANCES FOR HIGH DENSITY DISCHARGES

Radial power balances for three representative high density discharges with neutral beam injection have been constructed. Their trajectories in $1/q$ v $\bar{n}_e$ R/B_T space (Figure 1) show that they approach the high density limit.

3.1 Input data and method of analysis

The time dependence of the main plasma parameters and profiles of n_e and T_e obtained by fitting analytic forms to the Thomson scattering data are shown in Figures 3,4,7,8,10,11 and are summarised in Table II. Only central ion temperatures are estimated by analysis of charge exchange neutrals and/or neutron fluxes. Profiles of T_i are calculated, as outlined below. The least accurate of the input data are the total radiation and neutral density. Fortunately, these do not strongly affect the power balance near the centre of the discharge. The uncertainty in total radiation arises from the expected localisation near the injected neutral beams of enhanced radiation due to charge exchange recombination [21]. Since the field of view of the total radiation measurements does not intersect the neutral beams, this effect is approximately allowed for by increasing the measured radiation loss by a factor $\lesssim 2$. The central neutral density, $n_D(0)$ is not measured, so the analysis is repeated for various assumed values. The minimum value taken is zero and the maximum value is chosen by comparison with previous experiments with neutral beam heating, where $n_D(0)$ was estimated by a variety of techniques [22]. Specifically, $n_D(0) = 2 \times 10^{14}$ m^{-3} for discharge I and 5×10^{13} m^{-3} for discharges II and III. Neutrals arising from the injected beams are not treated separately.

The electron power balance and the distribution of injected power between ions and electrons is first calculated with an assumed profile for T_i using the time-dependent 'Hermes' transport analysis code [23]. This calculates neutral beam deposition and slowing down but does not make corrections for the displacement of the fast ion orbits from magnetic surfaces. The Stott neutral code [24] is used

to evaluate the neutral density profile assuming all neutrals originate at the plasma boundary with an energy of 10eV. Finally, the ion energy balance is completed using an ion transport code [25] which assumes conduction of the form given by Hazeltine and Hinton [26] but enhanced by a factor, K sufficient to balance the power input with conduction, convection and charge exchange losses. The profile of T_i thus obtained is reinserted in the electron power balance and the whole process repeated until a self-consistent result is achieved. It is found that the power loss by convection is generally $\lesssim$ 10% of the conducted power loss for both ions and electrons. In the power balances presented below this has not been separately distinguished and is included in the 'conduction' term.

3.2 Results

The power balances obtained from the analyses outlined above are illustrated in Figures 5,6, 9 and 12. The shaded areas in these figures indicate the uncertainty introduced by the range of assumptions about $n_D(0)$ and radiation losses, which are serious only at the edge of the discharge. The power balances in the central region are more accurate because of the weak influence of charge-exchange and radiation and because the central ion temperature is known. Estimates of electron thermal diffusivity, χ_e can be made for $r/a \sim 0.3$-0.7, where both the power balance and $\partial T_e/\partial r$ are known with reasonable accuracy. $n_e\chi_e$ is found to be a weak function of radius.

The main features of the results for the three discharges shown are as follows:

Discharge I - In the ohmic phase where equipartition is important we find K in the range 1-4 and $n_e\chi_e$ in the range 0.5 - 2.5 x 10^{19} m^{-1} s^{-1}.

$T_e - T_i$ is not sufficiently well known in this case, and so the transport coefficients cannot be determined precisely. With injection equipartition is much less important, ion and electron losses are comparable, and we obtain $K \sim 2\text{-}4.5$ and $n_e\chi_e \sim 3.5\text{-}5.0 \times 10^{19}\ m^{-1}\ s^{-1}$. That is the electron conduction losses have worsened with injection.

Discharge II - The ohmic phase is similar to the discharge in ref [11]. Injection produces an increase in both T_e and T_i, which is maintained as the density rises. There is no disruption in this case until after the neutral beam injection pulse. Strong sawteeth are seen on the soft X-ray signals. The power balance analysis shows that ion conduction is the dominant loss process at $r/a = 0.5$ and is insensitive to assumptions about $n_D(0)$ giving $K = 3\text{-}3.5$ and $n_e\chi_e \sim 3 \times 10^{19}\ m^{-1}\ s^{-1}$.

Discharge III - In this case the major radius was moved to 1.25m and the discharge limited on the outer edge only by the fixed Ti limiter. The two injection lines were fired at an interval of 40ms to avoid disruption caused by the disturbance to the equilibrium. A disruption usually followed the end of the injection pulse from the first beam line. The power balance gives $K \sim 1.5$ and $n_e\chi_e \sim 8 \times 10^{19}\ m^{-1}\ s^{-1}$, a factor 2-3 times greater than for the full aperture discharges. To have $n_e\chi_e \sim 3 \times 10^{19}\ m^{-1}\ s^{-1}$ would require a 3-fold increase in radiation losses or a much larger electron-ion equipartition, implying $T_i(0) \sim 250$ eV. This is not consistent with the measurements of neutron flux and would require $K \sim 8$.

3.3 Discussion

In the high density regime covered by the examples above, ion and electron conduction losses dominate the central region of the discharge. Typically the ion conductivity is enhanced by factors up to 4 times the Hazeltine-Hinton values. $n_e \chi_e$ is approximately constant from r/a = 0.3-0.7 for a given discharge but varies from $\sim$ 2-8 x 10^{19} m^{-1} s^{-1} in the different cases. Although the values of conductivity appear to increase somewhat during injection, the changes are no larger than the range of variations between different discharges. There is no clear evidence for any new loss process associated with the use of neutral beam injection for heating.

4. SCALING OF β AND τ_E AT HIGH DENSITY

4.1 Introduction

High density discharges are particularly interesting because long confinement times and thus, with high power auxiliary heating, high values of beta are expected. Taking the simple scaling $\tau_{Ee} = 5 \times 10^{-21} \bar{n}\, a^2$ [27] with $T_i \simeq T_e$ gives

$$\bar{\beta}_T(\%) \simeq 8.5 \times 10^{-20} \frac{\bar{n}_e \times P_{TOT}\,(MW)}{R\, B_T^{\,2}} \qquad \ldots (4.1)$$

Thus, for discharge II, equation (4.1) gives $\bar{\beta}_T \sim 1.5\%$ whereas the measured value is $\bar{\beta}_T \simeq 0.8\%$. Evidently, equation (4.1) is not an adequate description of the data. In this section the scaling of $\bar{\beta}_T$ (derived from the diamagnetic loop) with $\bar{n}_e$, P_{NI}, I_p and B_T is examined in turn and, finally, a relationship which is a better description of the data than equation (4.1) is derived.

4.2 Scaling of $\bar{\beta}_T$ with $\bar{n}_e$ and P_{NI}

In discharge II, the density is ramped throughout the injection pulse. However, β_T is not sensitive to the density ramp rate. Figure 13 shows its variation with density for this and other similar discharges with injection powers from 220kW to 860kW. At low density $\bar{\beta}_T$ increases with density, but at higher densities it goes through a maximum $\bar{\beta}_T(\max)$ and then declines slightly as the density limit $\bar{n}_e(\max)$ is approached. For $200 < P_{NI} \leq 600$kW both $\bar{n}_e(\max)$ and $\bar{\beta}_T(\max)$ increase with P_{NI}, but for $P_{NI} \geq 600$kW and $\bar{n}_e \geq 5 \times 10^{19}$ m^{-3} $\bar{\beta}_T$ changes very little as either P_{NI} or $\bar{n}_e$ are increased. This kind of behaviour, in disagreement with equation (4.1), was first reported in references [10, 22,28]. Figure 14 shows the variation of $\bar{\beta}_T(\max)$ with P_{NI} for this series of discharges. The scatter in the experimental data is such that the description of the behaviour at the highest injection powers must remain tentative in this case.

Figure 15 shows the variation of $\bar{\beta}_T$ with injection power P_{NI} and with total power P_{TOT} for a series of discharges, similar to discharge I, where B_T, I_p are kept constant and data is taken at the same density. Again, it is not possible to distinguish between a linear dependence of $\bar{\beta}_T$ on P_{NI} and a dependence which tends towards saturation at the highest powers. However, the dependence of $\bar{\beta}_T$ on P_{TOT} is clearly not linear.

4.3 Scaling of $\bar{\beta}_T$ with I_p and B_T

The region in which $\bar{\beta}_T$ is a weak function of density occurs on the right hand side of the operating diagram of Figure 1 where $\bar{n}_e \geq \frac{1}{2}\bar{n}_e(\max)$. Thus it is not possible to examine the variation of $\bar{\beta}_T$ with either I_p or B_T if all other parameters are kept fixed. However, Figure 16 shows the variation of $\bar{\beta}_T(\max)$ with I_p at four values of B_T, 0.9T, 1.35T, 1.8T

and 2.7T. At constant B_T, $\bar{\beta}_T$(max) increases strongly with current and at constant I_p, $\bar{\beta}_T$(max) increases strongly as B_T is decreased. At constant q, $\bar{\beta}_T$ is a weak, decreasing function of B_T. This behaviour can be approximated by β_p = constant $\simeq$ 1.0. However, $1.5 \lesssim \beta_p \lesssim 2.0$ can be achieved for $B_T \lesssim 1.35$T and $q \gtrsim 3.0$, whereas at B_T = 2.7T, β_p is usually less than 1.0.

4.4 Scaling laws for β_p, β_T and τ_E

In order to describe the parametric dependences more precisely, data from 264 discharges is analysed, for which conditions were deliberately varied over a wide range; B_T from 0.9 to 2.7T, I_p from 40 to 260kA, P_{NI} from 0 to 1MW, n_e from 2×10^{19} to 1×10^{20} m^{-3} and 'a' from 0.12 to 0.27m using both carbon and titanium limiters. β_p, $\bar{\beta}_T$ and τ_E are estimated from the diamagnetic loop signal. Each of these variables is then fitted to a power law in the other discharge variables $\bar{n}_e$, B_T, q, P_{TOT} and 'a' following the procedure described in reference [29] to obtain the results given in Table III, where P_{TOT} is in MW, and

TABLE III

SCALING LAWS FOR DITE DATA

Dependent variable	Constant Multiplier	Exponents of independent variables and standard deviation					Correlation coefficient	
		$\bar{n}_e$	B_T	q	P_{TOT}	a		
β_p	0.11 ± 0.1	0.44 ± .03	-0.83 ± .06	0.64 ± .05	0.23 ± .02	-0.73 ± .07	.82	... (4.2)
β_T%	7.3 ± .7	0.45 ± .03	-0.83 ± .05	-1.30 ± .04	0.25 ± .02	1.18 ± .06	.963	... (4.3)
τ_E(ms)	(1.1 ± .01) x 10^3	0.45 ± .03	1.17 ± .05	-1.33 ± .05	-0.76 ± .02	3.20 ± .06	.965	... (4.4)

Correlation coefficient and standard deviation are defined in reference [29]
Note that these equations are consistent

$\bar{n}_e$ in units 10^{19} m^{-3}. The major radius is not included as an independent variable because its range is too small. The uncertainties in the indices are less than 10%. These three fits to the data are illustrated in Figures 17, 18 and 19. Data from both ohmic discharges and injection dominated discharges are well described by these forms. The dependences on $\bar{n}_e$, B_T and q are qualitatively similar to those already described in the scaling experiments in sections 4.2 and 4.3. The dependence on power indicates that both $\bar{\beta}_T$ and β_p increase less rapidly with power at high total power input and that τ_E decreases as the total power input is increased. The curves superimposed on the data in Figures 14 and 15 follow equation (4.3) and though the data in Figures 14 and 15 (a) can equally well be described by a linear dependence on P_{NI}, Figure 15 (b), with P_{TOT} as abscissa, clearly supports equation (4.3).

A comparison of the DITE scaling for β_p with data from ohmically heated tokamaks ALCATOR-A [30], TFR [15], FT [16], ASDEX [31] and TOSCA [32] and from injection heated tokamaks ISX-B [2,33], T11 [20], JFT-2 [18] and PLT [34] is shown in Figure 20. It can be seen that equation (4.2) describes this data rather well without the need to introduce a major radius dependence. In addition, data from ohmically-heated and injection-dominated CLEO-stellarator plasmas [35] has been included in Figure 20. In this case we define $q = q_T$, $\beta_p = (R/a)^2 \, q_T^2 \, \beta_T$, where $1/q_T$ is the sum of the rotational transforms due to the ohmic current and the external helical windings. This suggests that q in equations (4.2) to (4.4) represents the geometrical confinement properties of the magnetic field rather than the plasma current as such. Recent data from ISX has given a scaling of the form $\beta_p / q^{1/2} \sim P_{NI}^{1/3}$, which is very similar to equation (4.2) [33].

4.5 Discussion

The behaviour of high beta injection dominated tokamak plasma is not consistent with relations of the form $\tau_E \sim na^2$. The scaling experiments in Sections 4.2 and 4.3 and the global description of Section 4.4 show a more complicated behaviour. The latter is consistent with data from ohmic discharges and neutral injection dominated discharges in DITE and other tokamaks. There is no reason to suppose that the behaviour is specific to neutral injection as a heating method, although this possibility cannot yet be excluded.

The dependence of τ_E on the mean diamagnetic temperature $\langle T \rangle = \langle T_e + n_i T_i / n_e \rangle$ can be found by substituting $P_{TOT} = \tau_E$ x energy content in equation (4.4). A strong inverse dependence of the form $\tau_E \sim \langle T \rangle^{-3.4 \pm 0.4}$ is implied. This suggests an unfavourable dependence of conduction losses on temperature or a decrease in confinement with increasing β.

5. THE DENSITY CLAMP

5.1 Description of the phenomena

The increment in density produced by beam refuelling in low density discharges approximately corresponds with the $\dot{n}(r)$ profile [36]. At higher densities, with a gettered vacuum vessel where the density is maintained or slowly increased by cold gas feed, the density increase produced by injection is often followed, after an interval of 3-20ms, by a sharp reduction in $d\bar{n}_e/dt$. The gas feed rate must be increased typically by a factor of 2-3 times in order to recover the preinjection value of $d\bar{n}_e/dt$. This effect is phenomenologically similar to the 'density clamp' reported on ISX-B [2].

No evidence for instabilities associated with the onset of the clamp has been seen using our present diagnostics, which have bandwidths up to ~ 20kHz. These include soft X-ray diodes viewing chords from R = 1.11m to 1.27m, coils inside the vacuum vessel in the shadow of the limiter and Langmuir probes in the scrape-off plasma. There is usually a small reduction in β_p compared with discharges in which the clamp is absent but this is consistent with only a few percent reduction in τ_E.

Fluctuations in density appear on the 2mm microwave interferometer traces after the onset of the clamp, with amplitude, $\Delta\bar{n}/\bar{n} \lesssim 5\%$ and $f \gtrsim$ 10kHz, as shown in Figure 21. These coincide with magnetic fluctuations at the plasma boundary which, however, show no regular structure with poloidal mode numbers in the range $1 \lesssim m \lesssim 4$.

A density clamp is almost always observed for discharges with 3 <

$q < 7$ and $0.2\ \bar{n}_{max} < \bar{n}_e < \bar{n}_{max}$ (where $\bar{n}_{max}$ is the density limit) when the torus is clean. The density does not appear to clamp if $q < 3$, which may be associated with the presence here of strong density sawteeth. The clamp can occur with both co- and counter-injection and with both deuterium and helium plasmas. It is sensitive to the major radial position of the plasma. When the discharge is moved 80mm inwards to R = 1.09m so that the plasma contacts the limiter on the inside edge the severity of the effect increases and it is very difficult to raise $\bar{n}_e$ even with a massive increase in gas feed. On the other hand moving the discharge out to R = 1.25m weakens or eliminates the effect. The major radial position is also found to affect the gas feed rate required to maintain the density in an ohmic discharge, with much smaller feed rates being required when the plasma is displaced outwards and larger feed rates required when the plasma is moved inwards. These results indicate that the clamp is associated with changes in the discharge boundary.

5.2 Global particle balance

The particle balance equation for plasma electrons can be written:

$$\frac{dN}{dt} = S - \int \Gamma \, ds \qquad \ldots (5.1)$$

where N is the total number of electrons in the discharge, S is the rate of production by ionisation and Γ is the particle flux across the plasma-wall interface. The integral is taken over the entire surface of the plasma. The particle confinement time is given by $\tau_p = N/\int \Gamma \, ds$.

The ionisation source term can be split into two components:

$$S = Sg + Sr$$

where Sg is due to cold gas feed and Sr is due to recycling of neutrals at the wall.

$$Sr = R_w \int \Gamma \, ds$$

where R_w is the recycling coefficient. Equation (5.1) then becomes

$$\frac{dN}{dt} = Sg - (1 - R_w) \int \Gamma \, ds \qquad \ldots (5.2)$$

A decrease in $d\bar{n}_e/dt$ does not necessarily imply a decrease in dN/dt if there is a transient change in the density profile. However, a transient effect would not account for the new equilibrium with reduced $d\bar{n}_e/dt$ or the need to increase Sg to maintain $d\bar{n}_e/dt$ at its preinjection level. A sustained reduction in $d\bar{n}_e/dt$ at constant gas feed or a constant $d\bar{n}_e/dt$ with increased gas feed then implies an increase in $(1 - R_w) \int \Gamma \, ds$.

In ohmic discharges we expect $R_w \simeq 0.5$ for deuterium and $R_w \simeq 0.9$ for helium [37]. To account for the magnitude of the density clamp seen in deuterium and helium discharges would require a fall in R_w of about 0.25 in each case. Although we expect R_w to fall as the edge temperature rises on injection, a fall of this magnitude requires the mean particle energy incident at the wall to increase from 50eV to about 1keV. This is clearly unreasonable and we conclude, in agreement with reference [38], that changes in recycling coefficient are too small to explain the density clamp phenomenon, and, consequently, an increase in $\int \Gamma \, ds$ is expected.

5.3 Observations in the scrape-off layer during the density clamp

Figure 21 shows Langmuir probe measurements of density and electron temperature at the limiter minor radius r = 0.26m for two discharges

which exhibit a density clamp following neutral injection and for a companion ohmic discharge with a similar gas feed rate. During neutral injection the edge temperature increases by a factor of between 1.5 and 2.0 and, after the onset of the density clamp, the edge density remains approximately constant.

The time resolved deuterium flux in the scrape-off layer parallel to B_T has also been measured with a rotating disc [8]. Figure 22 shows I, $\bar{n}_e$, dN/dt (assuming a constant n_e profile) and Γ measured at r = 0.27m for a discharge with neutral injection where the gas feed is kept constant. The clamp occurs 15ms after the start of neutral injection where Γ has increased by a factor ~ 2. A similar relative increase is seen with the disc at r = 0.255m suggesting that there is no change in the scale length for particle flux in the scrape-off layer during neutral injection. If these local measurements of Γ are representative, then $\int \Gamma \, ds$ has also increased by an amount which is consistent with the measured reduction in dN/dt without requiring changes in R_w or Sg. However, the measurements are not sufficiently accurate to exclude a small change in the recycling coefficient.

5.4 Discussion of observations on the density clamp

Since neutral beam injection produces electron and ion heating, we do not expect, a priori, that the particle confinement time will remain unchanged. Either a direct dependence of the diffusion coefficient on temperature or an outward redistribution of the electron source term due to a reduction in the mfp for ionisation would reduce τ_p. It should be noted that the global particle confinement time is most sensitive to conditions near the plasma boundary, where the electron source term is largest, especially at high density.

The measured changes in the parameters of the scrape-off plasma are consistent with a collisionless model in which the sheath between the scrape-off plasma and the limiter determines the boundary conditions for particle and energy flow. In this case the particle flux along $\underline{B}$ to the limiter surface is proportional to $n_e T_e^{\frac{1}{2}}$ and the corresponding energy flux, Q to $n_e T_e^{3/2}$. An increase in Q caused by an increase in heat input to the core plasma requires increases in Γ or T_e. In fact, both are observed. The increase in Γ and slight reduction or levelling off in n_e are thus seen as the plasma response to the new boundary conditions implied by additional heat conduction to the limiters.

In conclusion, the density clamp phenomenon appears to be associated with a fall in global particle confinement time which is consistent with the changes in the boundary layer brought about by the additional heat input. It is possible that an increase in the diffusion coefficient in the confined plasma is necessary to explain the reduction in τ_p. However, the observed fluctuation level increases only after the onset of the clamp and does not appear to be directly associated with it.

6. DENSITY LIMIT

The disruption which occurs as the density is raised was recognised early as a serious problem for tokamaks [39]. In plasmas contaminated with low-Z impurities such as O and C it has been convincingly shown that the disruption is preceded by a collapse of the current channel induced by over-cooling of the plasma periphery by impurity radiation [40,41]. This explanation was also supported by the scaling studies of Murakami et al. [42], and appeared to be confirmed by the increase of the density limit by removal of low-Z contaminants by gettering [43,3] or intensive

discharge cleaning [44,20]. The data from a wide range of tokamaks compiled by Pfeiffer and Waltz showed the same general trend of an increase in n_e(max) as Z_{eff} is reduced [45]. The picture was further confirmed by the extension of the density limit in contaminated discharges, in Ormak [46] and DITE [47] by additional neutral beam power, which can compensate to some extent the radiation losses.

On the basis of these results, it was expected that neutral beam injection would allow a considerable extension of the limit obtained in a gettered torus with ohmic heating. However, as shown in Figure 1 very little improvement is obtained at $q_L \gtrsim 4$ and the density reached with injection at $3.5 > q_L > 2$ appears to be an extension of the ohmic limit at higher q_L. These results suggest a maximum density, $n_{max} \sim I_p/a^2$ for $q_L > 2$ which is independent of the method of plasma heating and of the power input.

6.1 Density limit in low-Z contaminated discharges

In order to test the effectiveness of neutral beam injection in overcoming the density limit associated with low-Z impurities some work was done with the torus in an ungettered state after it had been opened to the atmosphere. In this case conditioning is achieved with short pulse and glow discharge cleaning to give Z_{eff} in the range of 3-4. The density limit with ohmic heating is a factor of 2.5 less than that in a gettered torus at $q_L \sim 5$ and similar to that reported previously [3]. With injection, a factor of 2 improvement is obtained, as shown in Figure 23. The maximum density increases with injection power level up to approximately 80% of that obtained in a gettered torus.

The effect of neutral beam injection on the width of the temperature profile is illustrated by a series of discharges in which the

density is increased monotonically by cold gas feed. A 100ms 900kW pulse of neutral beam injection is applied starting at t = 80ms, just before the ohmic density limit is reached. The 2nd harmonic electron cyclotron radiation is monitored using the Fabry-Perot interferometer in fixed frequency mode, at frequencies corresponding to R = 1.03m, R = 1.17m (centre) and R = 1.35m. These measurements provide an approximate but continuous record of the width of the electron temperature profile which is illustrated in Figure 24, based on a triangular fit to the data. In the ohmic phase a slow narrowing of the profile is evident as the density limit is reached, sometimes leading to a minor disruption just before injection. After injection, the profile broadens and then narrows again as the density is increased further. Though crude, these measurements are confirmed by fitting profiles of the form $T_e(eV) = 20 + (T_{eo} - 20)(1 - r^2/a^2)^m$ to data obtained by Thomson scattering. The value of m changes from ~ 3 to 4 between 120 and 130ms, consistent with the electron cyclotron data. The broadening of the temperature profile produced by injection and the postponement of disruption to higher density are the most notable features of these discharges.

Local measurements of T_e and n_e in the scrape-off plasma using Langmuir probes allow the particle and energy flow to the limiters to be estimated on the assumptions that there is a classical sheath at the limiter surface and that the conditions in the scrape-off plasma are not strongly dependent on toroidal and poloidal angle. The estimated power flux to the limiters decreases in the ohmic phase, but increases again during injection [48].

Typically, the steady increase in density is halted by one or more minor disruptions each preceded by a fast-growing mode with m = 2 and

followed after about 10ms by a major disruption.

These results clearly show the beneficial effect of neutral beam injection on the density limit obtained in an ungettered torus, contaminated by low-Z impurities. It appears that the additional power counteracts the tendency of the current channel to contract as the density is raised, allowing the density limit to be improved by a factor of 2.

6.2 Density limit in a gettered torus

In DITE, the density limit in a gettered torus is also improved by neutral beam injection for $2 < q_L < 4$, as shown by curves B and C in Figure 1. However, in devices with very low levels of impurity, such as Alcator-A and Doublet III, Figure 2 shows that the region between curves B and C is also accessible with ohmic heating. At low-q, the discharge is apparently more sensitive to impurity effects and thus there is an improvement in $\bar{n}_e$(max) with additional heating, which helps to stabilise the m = 2 mode [22], as in the contaminated discharge discussed above.

For $q_L \geq 5$ the situation is completely different. Neutral beam injection produces no noticeable increase in the density limit, even when the total power input is increased by a factor of 5. In this case, the maximum density is proportional to the plasma current (or rather, the current density, as discussed in Section 6.4). It is insensitive to the additional power input and, by inference, would not be improved by a further reduction in impurity levels. The last two remarks also apply to the maximum density reached at low-q with modest amounts of additional heating, thus curve C in Figures 1 and 2 appears to be a new density limit which is insensitive to power input provided this is sufficiently large.

6.3 Precursors to disruption at high density

Measurements of poloidal field fluctuations invariably show a rapid increase just before disruption at high density. The dominant mode has m = 2 and a frequency of a few kHz. It typically grows from a level $\tilde{B}_p/B_p < 0.1\%$ in the 1ms period before the negative voltage spike and thus gives very little warning of disruption.

The data from soft X-ray diodes is somewhat variable. A chord viewing the discharge centre sometimes shows a rapid increase 10-20ms before disruption and a tendency for sawtooth oscillations to disappear as observed in the centre of the discharge in ohmically heated Pulsator with low gas feed rates and attributed to accumulation of impurities [19]. This is the commonest behaviour when counter-injection is used. In other cases, when the major disruption is preceded by one or more minor disruptions, these are like abnormally large sawteeth. The central chord signal is reduced and a corresponding, temporary increase in the signals from outer chords is observed. However, when attention is restricted to discharges which reach line C in Figure 1, the behaviour is more consistent, though statistics are rather sparse to draw general conclusions. In this case, as illustrated in Figure 25, sawtooth oscillations are superimposed on a slowly increasing or decreasing signal and continue up to the point of disruption. This is like the behaviour in Pulsator at the highest densities reached [19].

Finally, cine films taken at a framing speed of 3000 fps were examined for evidence of a contraction of the bright ring surrounding the discharge centre such as was observed on ATC tokamak [43]. Such a contraction is seen prior to disruption in an ohmic discharge if the torus is not gettered. However for the case of disruption in a gettered torus either with or without injection, though the thickness and brightness of the luminous boundary increases slightly as the density is

raised, there is no evidence of a contraction. However, on some films, the frame immediately preceding disruptions shows a distortion of the boundary layer which suggests the growth of a large magnetic island near the boundary ~ 0.3ms before disruption. Contractions of the luminous boundary can clearly be seen preceding each of the subsequent disruptions which usually terminate the discharge. In this case, the plasma is very likely to be strongly contaminated by impurities released from the walls in the first disruption of the series near the density limit.

6.4 Scaling of the density limit

The form of the stability diagram in Figure 1 suggests a maximum density which is primarily proportional to current density, but modified by the q value at the limiter. This has been confirmed over a range of toroidal field from 0.9 to 2.7T. The limit is only reached for $2 < q < 3$ with additional heating and $q < 2$ is not attained.

The sensitivity of $\bar{n}_e(\max)$ to mean current density has been checked by restricting the minor radius, either by moving the plasma inwards or outwards against the fixed Ti limiters or by the use of movable carbon limiters as described above. Keeping the plasma current and toroidal field constant, the integral $\int n_e \, d\ell$, as measured by a 2mm microwave interferometer, shows an increase proportional to a^{-m} with $0 < m \lesssim 1$. This suggests $\bar{n}_e(\max) \sim 1/a$ to $1/a^2$.

The increase in the maximum density achievable as the aperture is decreased is less when the carbon limiters are used. It is possible there is some current flow outside the limiter radius in this case.

The general features of the operating diagram of Figure 1 are preserved in these reduced aperture discharges, and in particular the

density limit scales linearly with ohmic current for a fixed minor radius. Figure 26 shows a log-log plot of the ratio $\int n_e \, d\ell / I_p$ versus minor radius. Here the minor radius is taken as the distance from the plasma centre, measured by electromagnetic diagnostics, to the nearest limiter surface. The scatter in the points represents a small shot to shot variation and a larger variation which depends on the choice of pre-programming of the gas valves, current and position. The highest densities obtained using titanium limiters are consistent with a scaling $\bar{n}_e(\max) \propto I_p/a^2$. The highest densities obtained using the carbon limiters suggest a weaker dependence on minor radius.

Further evidence on the scaling of $\bar{n}_e(\max)$ with I_p/a^2 is provided by the data from other tokamaks [2,12-20] summarised in Figure 2. These densities are not necessarily the highest achieved on a particular device but do cover the following range of parameters:

B_T = 0.3 to 9T

I_p = 20 to 600kA

$\bar{n}_e$ = 3.5 10^{19} to $\sim 10^{21}$ m^{-3}

R = 0.3 to 1.45m

a = .08 to .4m

6.5 Discussion

The factor of 2 improvement in the density limit which is produced by neutral beam injection into a discharge contaminated with low-Z impurities can be attributed to compensation of the radiation losses from the plasma boundary which normally lead to contraction of the temperature and current profile.

However, in a gettered torus, the density limit is not improved by an increase in power input, implying that impurity radiation is unlikely to be an intermediate cause of disruption in this case. The invariable

presence of a rapidly growing m = 2 mode before disruption indicates that the destabilisation of this mode is the primary cause of disruption. There is no evidence for a collapse of the current channel, though slow changes in the current density profile can not be ruled out. Calculations of the ballooning effect at the q = 2 surface for a particular case show that the pressure gradient is within a factor of 2 of that required to affect m = 2 mode stability [49]. However, no direct evidence for this driving mechanism has been obtained.

It is interesting that the density limit represented by line C in Figure 1 is close to the maximum density obtained in stable toroidal pinches for which $I/\pi n_e a^2 \sim 10^{-14}$ Am [50]. This suggests that a common explanation may be found for both configurations.

7. CONCLUSIONS

Detailed energy balances for high density discharges show that ion and electron conduction losses dominate the central region. At the edge of the discharge, electron conduction, radiation and charge-exchange are the most important loss processes. The measured ion thermal conduction coefficient is 1.5-3.5 times larger than the value given by Hazeltine and Hinton. $n_e \chi_e$ is a weak function of radius and its value varies from $\sim$ 2-8 x 10^{19} m^{-1} s^{-1} in different discharges. It is somewhat larger in the beam-heated phase than in the ohmic phase of the same discharge.

The scaling of τ_E is not consistent with the form assumed for INTOR ($\tau_E \sim na^2$). This is not surprising since no single loss process is dominant. The most noticeable effects are the increase in the energy content with plasma current and the weak dependence on density and power input. The general behaviour of τ_E and β_T in DITE is consistent with data from ISX, T11 and JFT2, though in our case the β-values are

below the stability threshold for high n, ideal ballooning modes.

The density clamp observed on injection corresponds with an increase in the flow of power and particles to the limiter and in T_e at the boundary. Further measurements are required to determine whether changes in the particle diffusion coefficient are required to explain this effect.

The maximum density reached with injection scales with mean current density. It is independent of injection power at high enough power and appears to be an extension of the high density limit obtained in ohmically heated discharges at high-q. The rise in density is terminated by a disruption preceded by a fast-growing m = 2 mode but the cause of the m = 2 mode destabilisation is not understood.

TABLE I: DIAGNOSTICS USED

Diagnostic Method	Parameters Evaluated	Ref.
Rogowski coil	Plasma current, I_p	
Toroidal loops	Loop voltage, V_ℓ	
Cosine and saddle coils	Discharge position	[4]
Diamagnetic loop	Poloidal beta, β_p	
Poloidal and radial fields of form $\cos(m\theta)$ with m=1,2,3	$\beta_p + \ell_i/2$, ellipticity and triangularity	[5]
16 B_θ coils inside the vacuum vessel	Amplitude and frequency of modes with m=1,2,3,4 sensitivity $\sim \pm 10^{-5}$T bandwidth $\sim$ 20kHz	
Soft X-ray diode array	Internal disruption and other instabilities near centre	
BF_3 counters with paraffin-wax moderation	Neutron flux, T_{io} with time resolution $\sim$ 10ms	
Thomson scattering	Profiles of n_e and T_e	[6]
2mm interferometer	$\int n_e \, d\ell$ across a central chord off-axis chords usually suffered refraction	
Mass-selecting neutral particle analyser with vertical scan at 15° to major radius	Profiles of T_i	
Radially movable, double Langmuir probes	n_e, T_e and scrape-off layer thickness. Power and particle fluxes to limiters	[7]
Rotating carbon disc collector	Time resolved deuterium flux in boundary layer	[8]
Total radiation scan using collimated thermopiles	Profile of radiated power per unit volume, after Abel inversion	
Spectroscopic measurements	Impurity behaviour	
Framing movie film at up to 3000 frames per second	Behaviour of boundary of hot core	
Electron cyclotron emission at $2\omega_{ce}$	Profile of T_e	[9]

TABLE II

SUMMARY DATA FOR DISCHARGES DESCRIBED IN SECTION 3

Title	I Discharge with $q \simeq 3.5$		II Low q discharge	III Reduced aperture
Shot numbers	16124-16145	16124-16145	16207-16227	18480-18489
Times (ms)	75	100	170	145
Ohmic current I_p (kA)	110	112	158	72
Loop voltage V_ℓ (V)	1.56	0.77	0.99	1.4
Toroidal field B_T (T)	1.35	1.35	1.35	1.9
Minor radius (m)	0.26	0.26	0.26	0.18
Major radius (m)	1.17	1.17	1.17	1.25
Limiter	Titanium	Titanium	Titanium	Titanium
Working gas	Deuterium	Deuterium	Deuterium	Deuterium
Injection power (kW)	0	680	620	850
q(a)	3.55	3.48	2.47	3.4
Electron temperature profile				
T_{eo} (eV)	462 ± 6	759 ± 11	743	634
p	1.0	1.0	1.0	.38
q	2.59	2.12	1.56	.81
Density profile				
n_{eo} (10^{19} m^{-3})	4.62	5.92	6.8	8.1
$\bar{n}_e$ (10^{19} m^{-3})	3.20	3.70	4.8	5.7
m	3.2	1.5	2.58	.43
n	7.0	2.75	2.79	.38
T_{io} NPA (eV)	200-300	577		470
T_{io} neutrons (eV)	-	570	555	470
Z_{eff}	1.2	1.5	1.65	1.3
β_p	0.62	1.1	0.8	1.6
$\hat{\beta}_T$ %	~ 0.45	1.74	2.0	1.0
$\bar{\beta}_T$ %	0.24	0.45	0.67	0.3
τ_E (ms)	24	10	14.5	5

Temperature profile $T_e(r) = (T_{eo} - 20)\left(1 - \left(\frac{r^2}{a^2}\right)^p\right)^q + 20$

Density profile $n_e(r) = 0.9\, n_e(0)\left(1 - \left(\frac{r^2}{a^2}\right)^m\right)^n + 0.1\, n_e(0)$

REFERENCES

[1] PAUL, J.W.M., AXON, K.B., BURT, J., CRAIG, A.D., ERENTS, S.K. et. al. in Plasma Physics and Controlled Nuclear Fusion Research (Proc. 6th Int. Conf. Berchtesgaden, 1976) IAEA, Vienna, Vol. II (1977) 269

[2] MURAKAMI, M., SWAIN, D.W., BATES, S.C., BUSH, C.E., CHARLTON, L.A. et. al. in Plasma Physics and Controlled Nuclear Fusion Research (Proc. 8th Int. Conf. Brussels, 1980) IAEA, Vienna, Vol I (1981) 337

[3] FIELDING, S.J., HUGILL, J., McCRACKEN, G.M., PAUL, J.W.M., PRENTICE, R. et. al. Nucl. Fusion 17 (1977) 1382

[4] HUGILL, J., GIBSON, A. Nucl. Fusion 14 (1974) 611

[5] WOOTTON, A.J. Nucl. Fusion 19 (1979) 987

[6] PRENTICE, R. Culham Laboratory Report CLM-R179 (1978)

[7] PROUDFOOT, G., HARBOUR, P.J. Journ. Nucl. Materials 93 & 94 (1980) 413

[8] ERENTS, S.K., HOTSTON, E.S., McCRACKEN, G.M., SOFIELD, C.J., SHEA, J. Journ. Nucl. Materials 93 & 94 (1980) 115

[9] BAKER, E.A.M. in Proc. 5th Conf. on Infrared and Millimetre Waves, Würzberg (1980)

[10] AXON, K.B., CLARK, W.H.M., CORDEY, J.G., COX, M., FIELDING, S.J. et. al. in Plasma Physics and Controlled Nuclear Fusion Research (Proc. 8th Int. Conf. Brussels, 1980) IAEA, Vienna, Vol I (1981) 413

[11] HUGILL, J., WOOTTON, A.J., AXON, K.B., POWELL, B.A., PRENTICE, R., SUMMERS, D.D.R., and WILSON, C.M., in Controlled Fusion and Plasma Physics (Proc. 9th Europ. Conf. Oxford, 1979) Culham Laboratory, Vol. I, (1979) 151.

[12] TOI, K., ITOH, S., KADOTA, K., KAWAHATA, K., NODA, N. et. al. Nucl. Fusion 19 (1979) 1643

[13] MEADE, D., ARUNASALAM, V., BARNES, C., BELL, M., BOL. K. et. al. in Plasma Physics and Controlled Nuclear Fusion Research (Proc. 8th Int. Conf. Brussels, 1980) Vol. I, IAEA Vienna (1981) 665.

[14] KITSUNEZAKI, A., FUJISAWA, N., IOKI, K., KONOSHIMA, S., NAGAMI, M. et. al. ibid. p405

[15] EQUIPE TFR, ibid. p425

[16] BARTIROMO, R., BRUSATI, M., BURATTI, P., CILLOCO, F., DE MARCO, F., et. al. ibid. p43

[17] FAIRFAX, S., GONDHALEKAR, A., GRANETZ, R., GREENWALD, M., GWINN, D. et. al. ibid. p 439

[18] SUZUKI, N., IMAI, T., FUJISAWA, N., MAENO, M., YAMAMOTO, T. et. al. ibid. Vol II (1980) 525

[19] ENGELHARDT, W., SESNIC, S., LACKNER, K., FUSSMANN, G., GERNHARDT, J. et. al. in Controlled Fusion and Plasma Physics (Proc. 9th Europ. Conf., Oxford, 1979) Culham Laboratory (1979) 88

[20] MUKHOVATOV, V.S., Proc. 2nd Joint Grenoble-Varenna Int. Symp. on Heating in Toroidal Plasmas, Como, Vol II (1980) 761

[21] CLARK, W.H.M., CORDEY, J.G., COX, M., FIELDING, S.J., GILL, R.D. et. al. Nucl. Fusion 22 (1982) 333

[22] HUGILL, J., Proc. 2nd Joint Grenoble-Varenna Int. Symp. on Heating in Toroidal Plasmas, Como, Vol II (1980) 775

[23] CORDEY, J.G., START, D.F.H., HUGHES, M., further details available on request

[24] STOTT, P.E., Plasma Physics 18 (1976) 251

[25] JOHNSON, P.C., further details available on request

[26] HAZELTINE, R.D., HINTON, F.L., Phys. Fluids 16 (1973) 1883

[27] INTOR Group, International Tokamak Reactor, IAEA, Vienna (1980)

[28] LOMAS, P.J., AXON, K.B., BRADLEY, J.E., GILL, R.D., HUGILL, J. et. al. in Controlled Fusion and Plasma Physics (Proc. 10th Europ. Conf., Moscow, 1981) Vol I, Moscow (1981) 1

[29] HUGILL, J., SHEFFIELD, J., Nucl. Fusion 18 (1978) 15

[30] COPPI, B., LAMPIS, G., PEGORARO, F., PERONI, L., SEGRE, S. MIT Report, PRR 7524 (1975)

[31] KEILHACKER, M., ALBERT, D.B., BEHRINGER, K., BEHRISCH, R., ENGELHARDT, W. et. al. in Plasma Physics and Controlled Nucl. Fusion Research (Proc. 8th Int. Conf. Brussels, 1980) IAEA, Vienna, Vol I (1981) 366

[32] CIMA, G., GOWERS, C.W., HARDING, G.E.S., KING, R.E., KRAUSE, H. et. al. in Controlled Fusion and Plasma Physics (Proc. 7th Europ. Conf. Lausanne, 1975) 1 Lausanne, (1975) 6

[33] SWAIN, D.W., MURAKAMI, M., BATES, S.C., BUSH, C.E., DUNLAP, J.L. et. al. Nucl. Fusion 21 (1981) 1409

[34] STODIEK, W., GOLDSTON, R., SAUTHOFF, N., ARUNASALAM, V., BARNES, C. et. al. in Plasma Physics and Controlled Nuclear Fusion Research (Proc. 8th Int. Conf. Brussels, 1980) IAEA, Vienna, Vol I (1981) 9

[35] LOMAS, P.J., JOHNSON, P.C., LEES, D.J., THOMAS, P.R., Proc. 2nd Joint Grenoble-Varenna Int. Symp. on Heating in Toroidal Plasmas, Como (1980) 849

[36] PAUL, J.W.M. in Controlled Fusion and Plasma Physics (Proc. 9th Europ. Conf., Oxford, 1979) Culham Lab. (1979) 371

[37] McCRACKEN, G.M., DEARNALEY, G., GILL, R.D., HUGILL, J., PAUL, J.W.M. et. al. Journ. of Nucl. Materials 76 & 77 (1978) 431

[38] HOWE, H.C., Journ. of Nuclear Materials 93 & 94 (1980) 17

[39] ARTSIMOVICH, A.A., Nuclear Fusion, 12 (1972) 215.

[40] HOSEA, J.C., BOBELDIJK, C., GROVE, D.J. in Plasma Physics and Controlled Nuclear Fusion Research (Proc. 4th Int. Conf. Madison, 1971) Vol II, IAEA Vienna (1971) 425

[41] JACOBSEN, R.A., Plasma Physics 17 (1975) 547

[42] MURAKAMI, M., CALLEN, J.D., BERRY, L.A. Nucl. Fusion 16 (1976) 347

[43] STOTT, P.E., DAUGHNEY, C.C., ELLIS, R.A. Nucl. Fusion 15 (1975) 431

[44] EQUIPE TFR in Controlled Fusion and Plasma Physics (Proc. 7th Int. Conf. Innsbruck, 1978) Vol I, IAEA Vienna (1979) 135

[45] PFEIFFER, W., WALTZ, R.E. Nucl. Fusion 19 (1979) 51

[46] BERRY, L.A., BUSH, C.E., CALLEN, J.D., COLCHIN, R.J., DUNLAP, J.L. et. al. in Plasma Physics and Controlled Nuclear Fusion Research (Proc. 6th IAEA Conf. Berchtesgaden, 1976) Vol II, IAEA Vienna (1977) 49

[47] AXON, K.B., BAXTER, G.A., BURT, J., CLARK, W.H.M., McCRACKEN, G.M. et. al. in Plasma Physics and Controlled Nuclear Fusion Research (Proc. 7th IAEA Conf. Innsbruck, 1978) Vol I, IAEA Vienna (1979) 51

[48] PROUDFOOT, G., HARBOUR, P.J. J. Nucl. Mater. 111 & 112 (1982) 44

[49] WESSON, J. details available on request

[50] BUFFA, A., COSTA, S., DE ANGELIS, R., GIUDICOTTI, L., GOWERS, C.W. et. al. in Plasma Physics and Controlled Nuclear Fusion Research (Proc. 8th Int. Conf., Brussels,1980) Vol I, IAEA Vienna (1981) 275

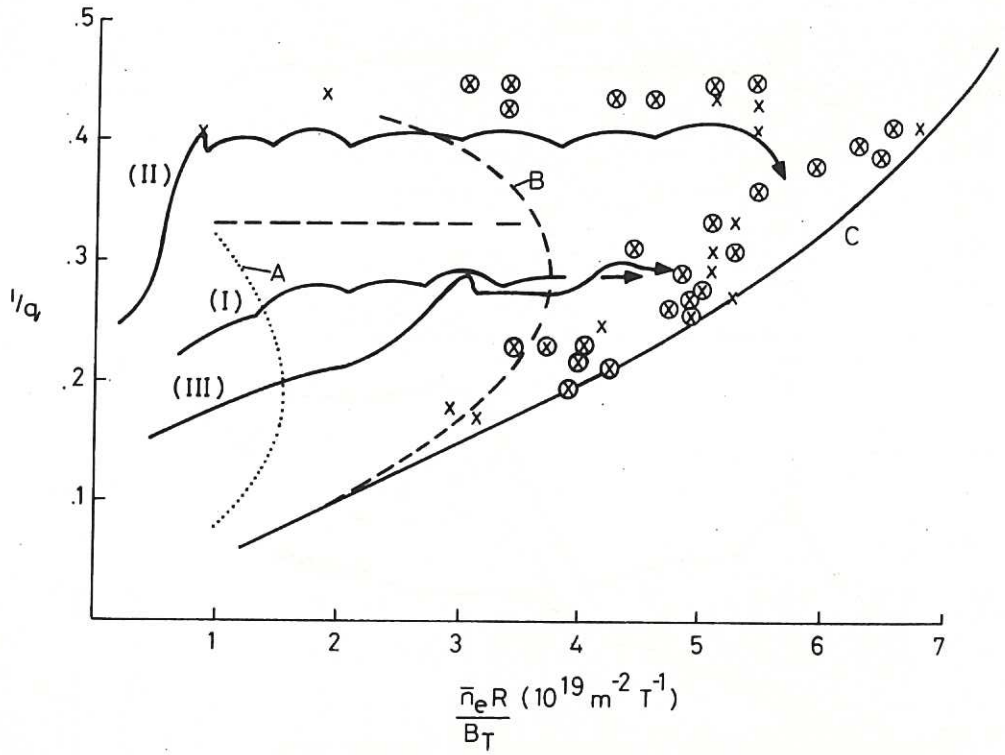

Fig.1 High density limit on 1/q versus $\bar{n}_e R/B_T$ space for various conditions: curve A, ohmic heating in ungettered torus [1]; curve B, ohmic heating in gettered torus; curve C, neutral injection heating in gettered torus. The trajectories labelled I, II and III correspond to the discharges in Table II.

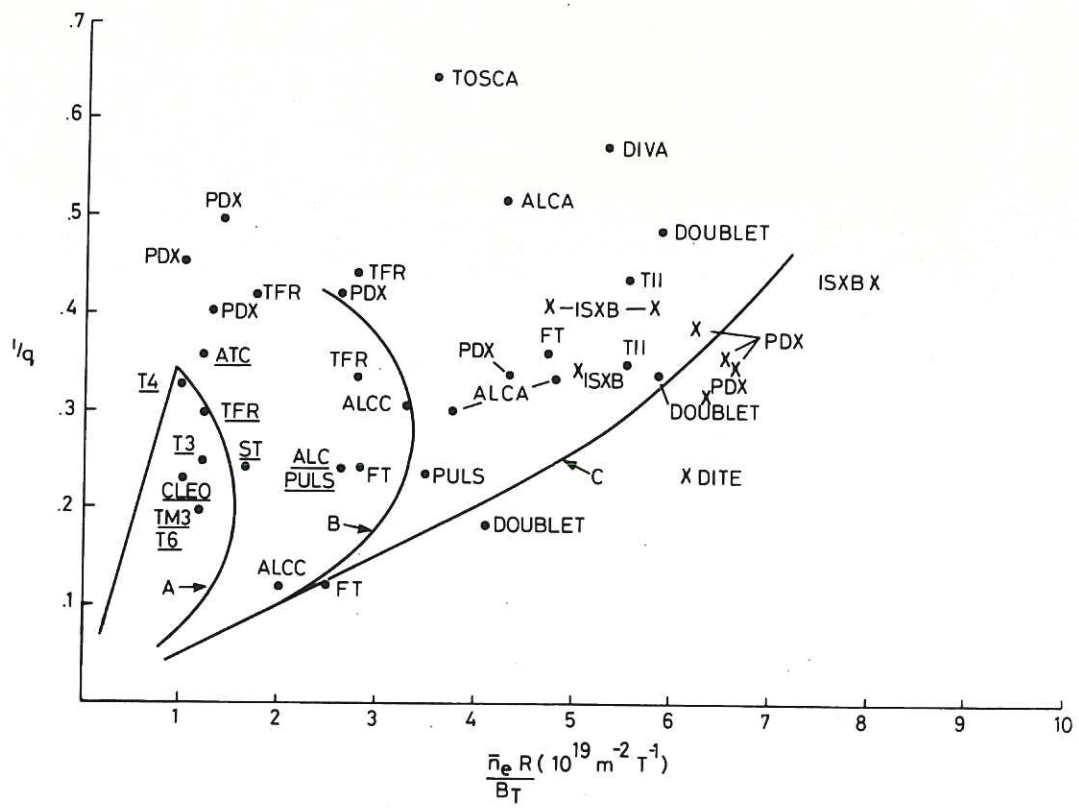

Fig.2 Data from other tokamaks superimposed on the DITE stability diagram. Data underlined refers to discharges considered by Murakami [42]. Solid circles – ohmic heating. Crosses – additional heating.

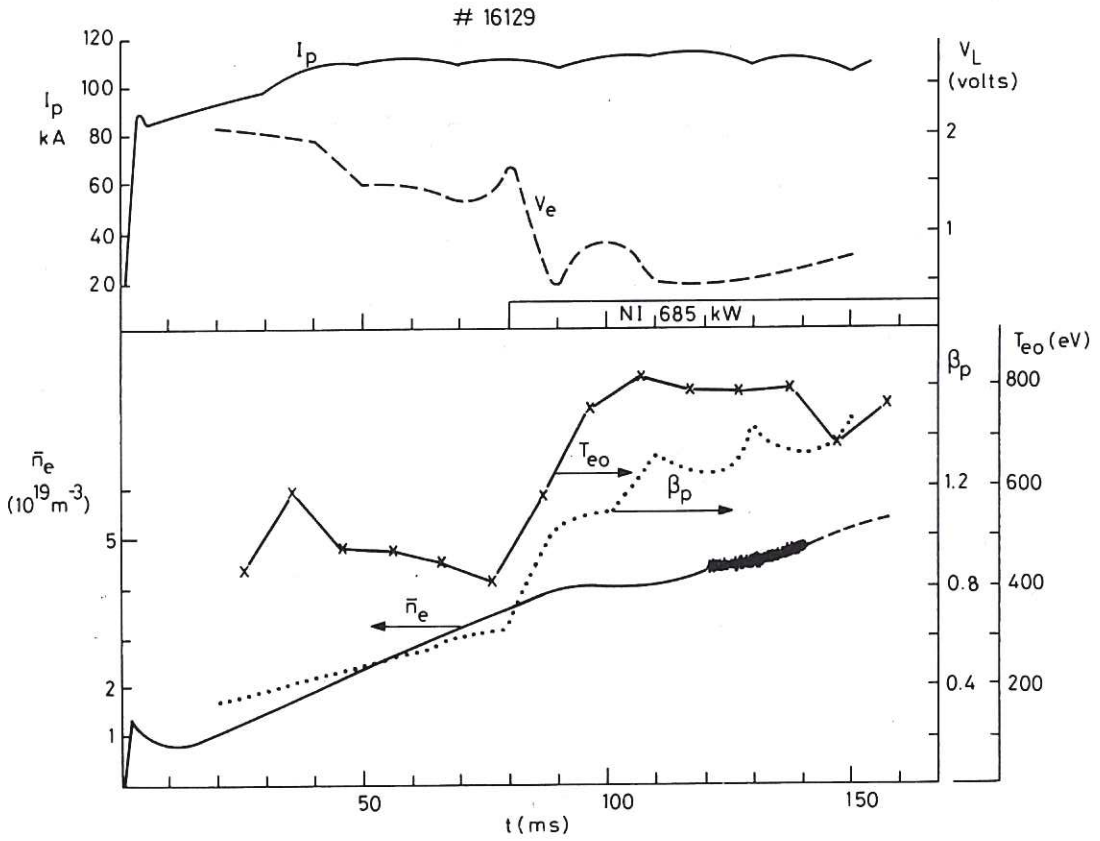

Fig.3 Time dependence of the main parameters for discharge I.

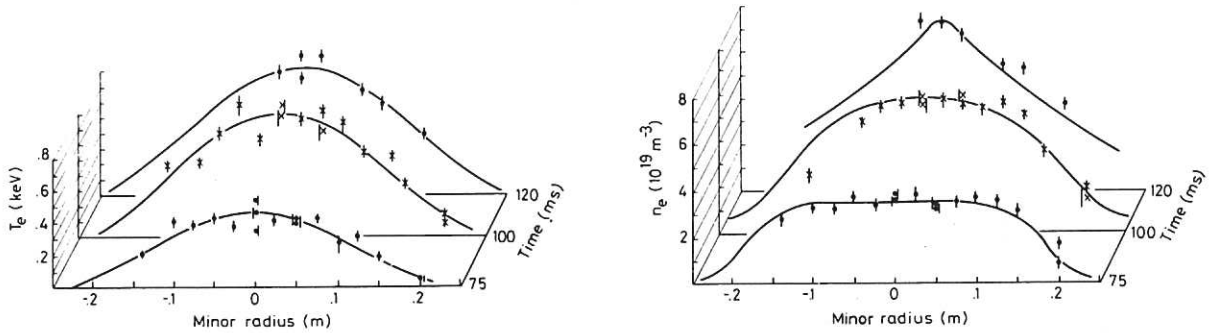

Fig.4 T_e and n_e profiles from Thomson scattering for times 75,100 and 120 ms into discharge I.

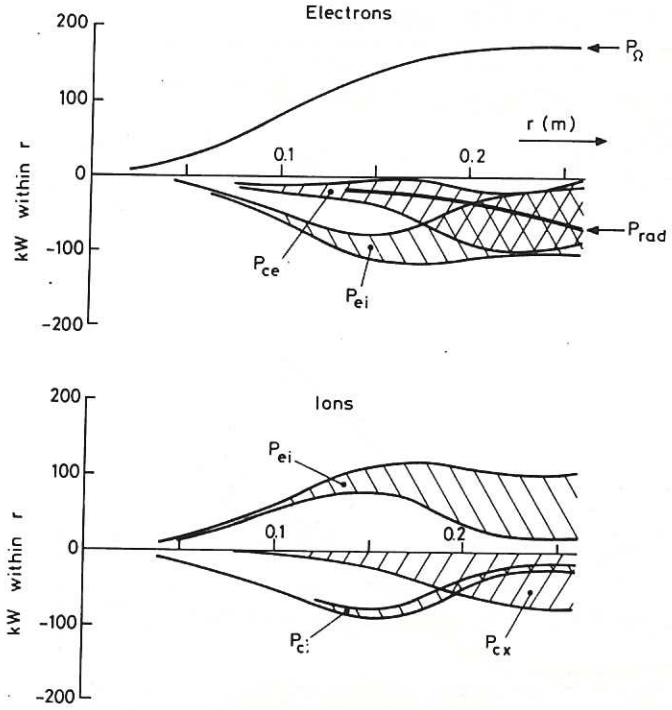

Fig.5 Radial power balance at time 75 ms into discharge I. P_Ω is the ohmic power input, P_{ei} is the equipartition power, P_{rad} is radiation, P_{ce} is electron thermal conduction and convection, P_{cx} is the charge-exchange loss from thermal ions and P_{ci} is the ion thermal conduction and convection loss. The shading refers to uncertainties in the analysis – see text. Inputs are shown positive and losses negative.

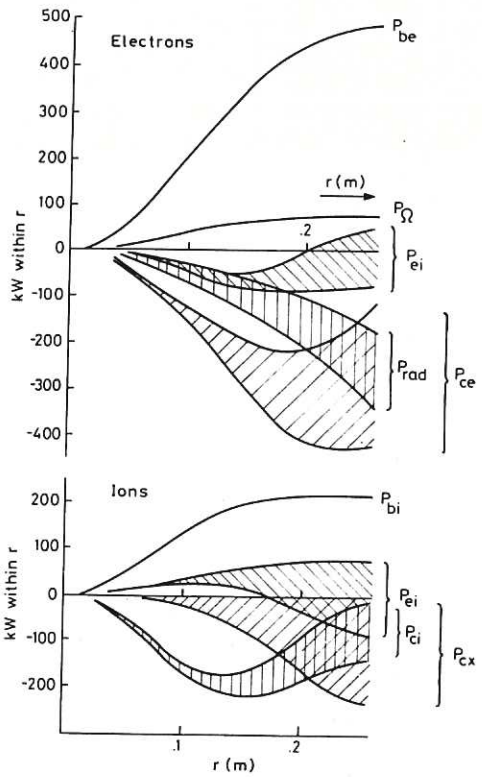

Fig.6 Radial power balance at time 100 ms into discharge I. P_{be} and P_{bi} are the beam inputs to electrons and ions respectively, other labels are as defined for Fig.5.

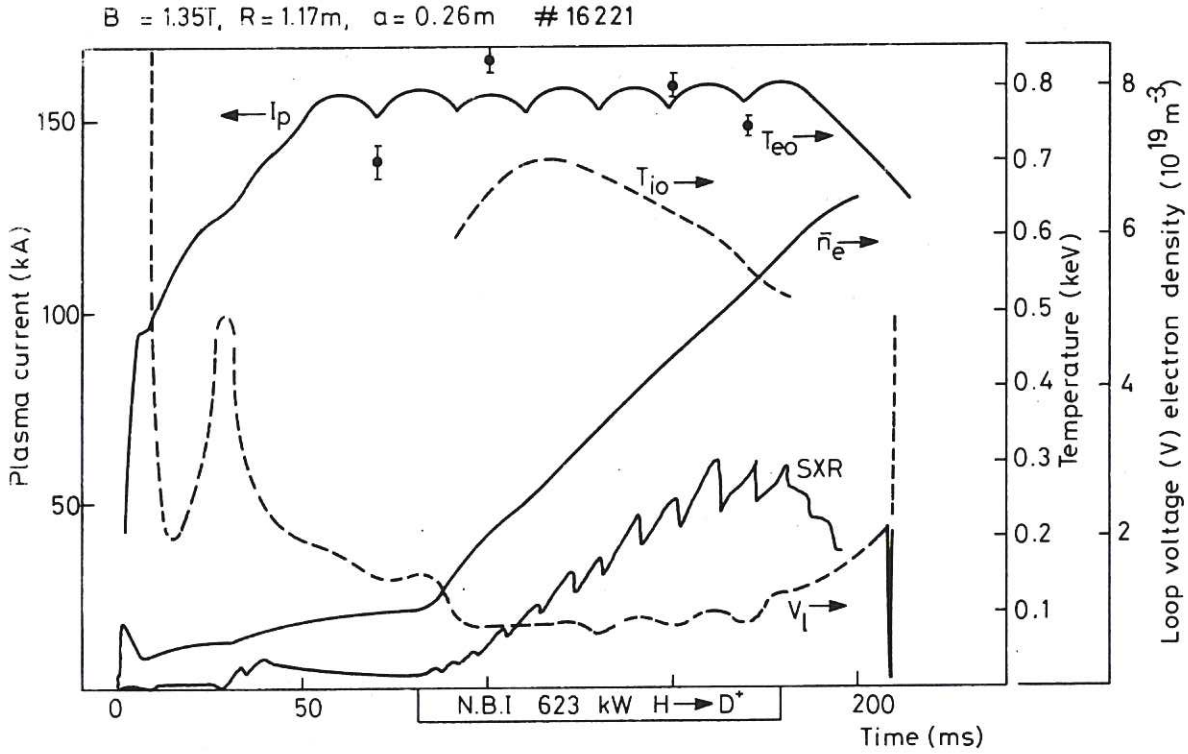

Fig.7 Time dependence of main parameters for discharge II.

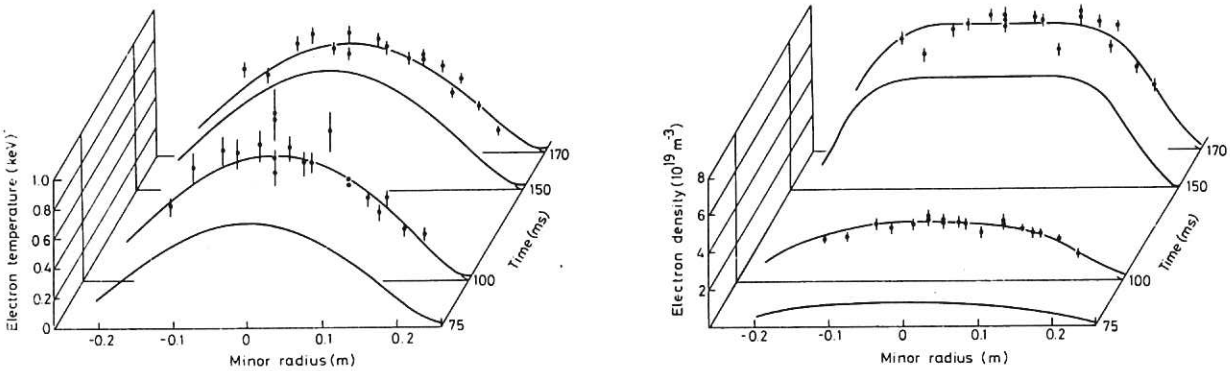

Fig.8 T_e and n_e profiles from Thomson scattering for times 75 ms, 100 ms, 150 ms and 170 ms into discharge II.

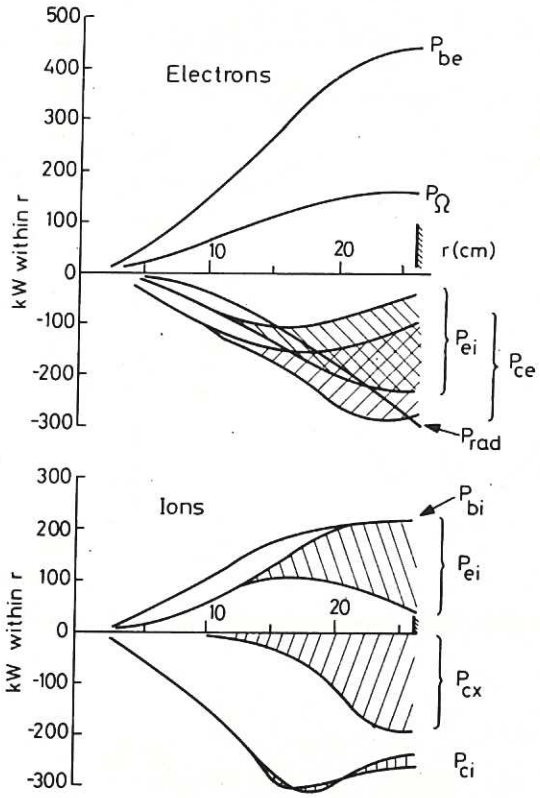

Fig.9 Radial power balance at time 170 ms into discharge II. Labels defined as in Figs.5 and 6.

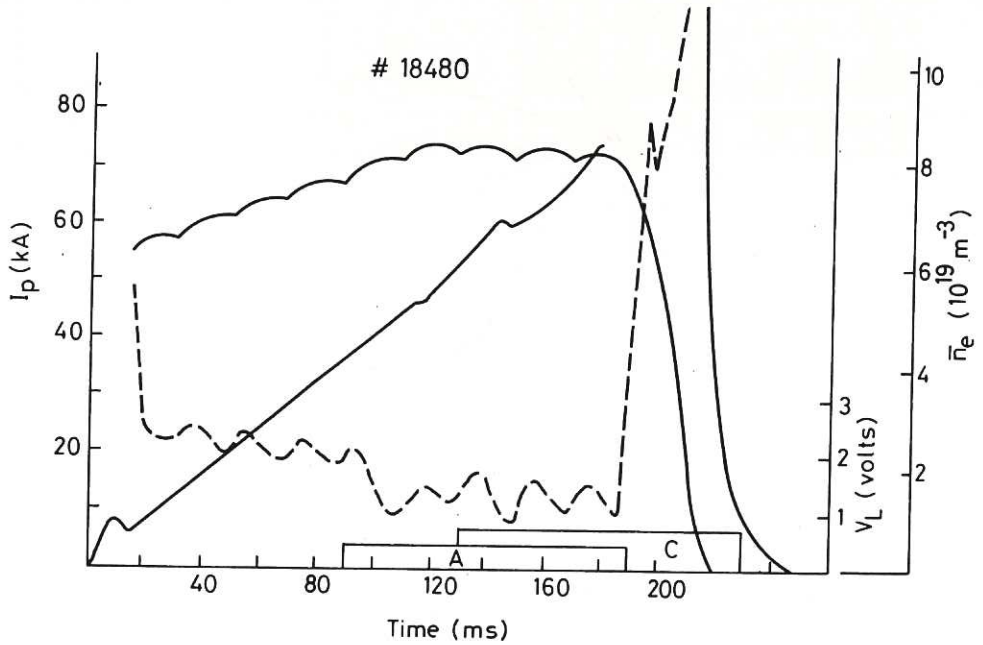

Fig.10 Time dependence of main parameters of discharge III.

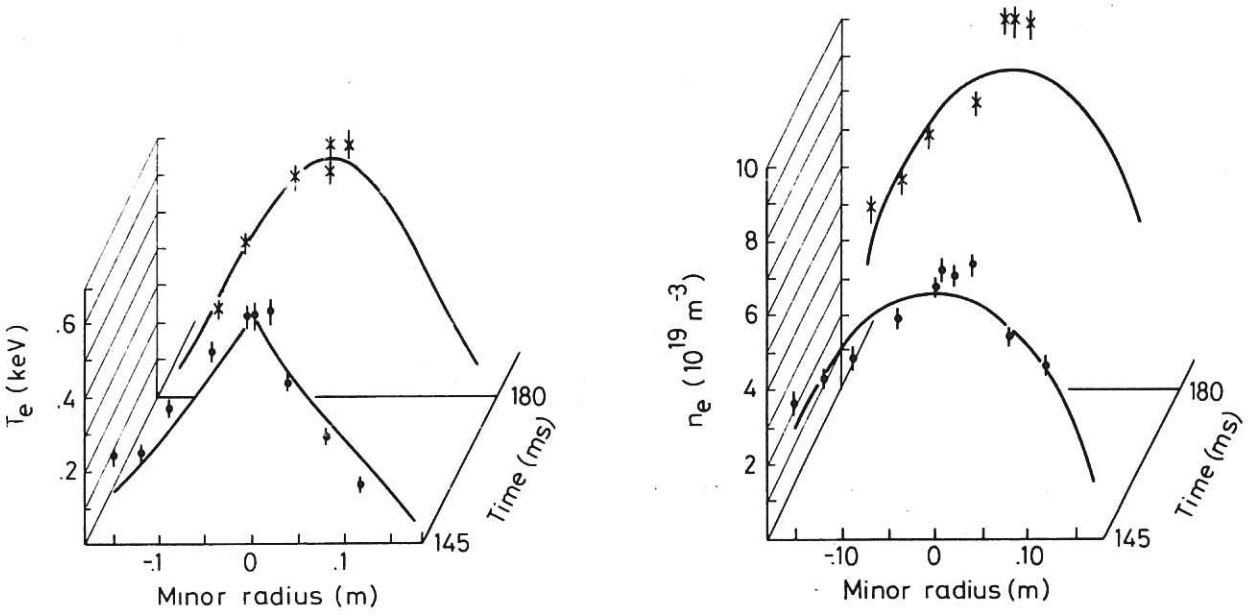

Fig.11 T_e and n_e profiles from Thomson scattering for times 145 ms and 180 ms into discharge III.

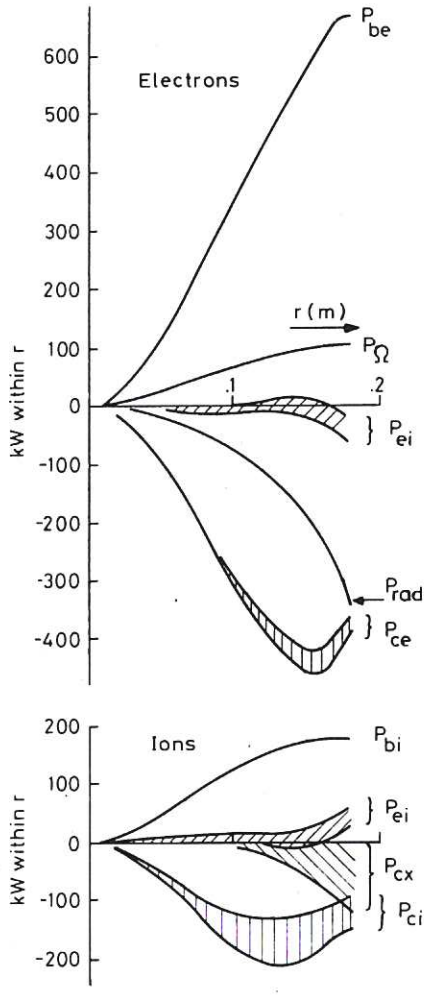

Fig.12 Radial power balance at time 145 ms for discharge III. Labels defined as for Figs.5 and 6.

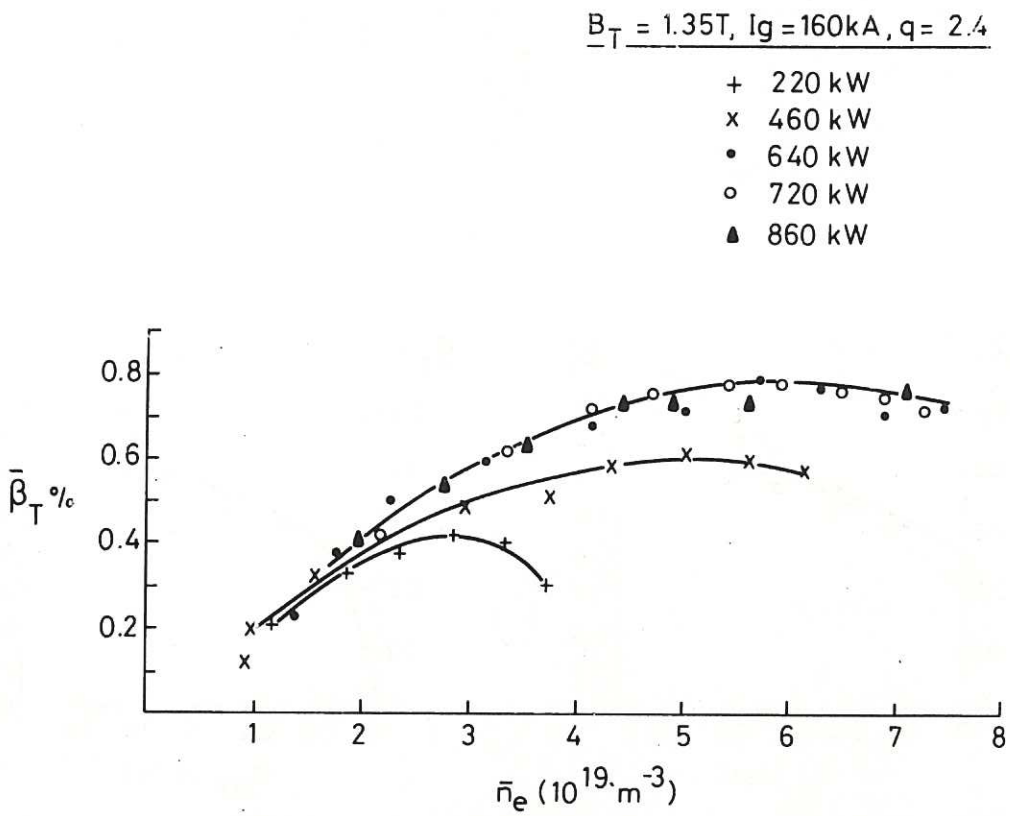

Fig.13 Mean toroidal beta, $\bar{\beta}_T$, from diamagnetic loop as a function of density for a series of discharges similar to Fig.7 but with various injection powers in the range 200–900 kW.

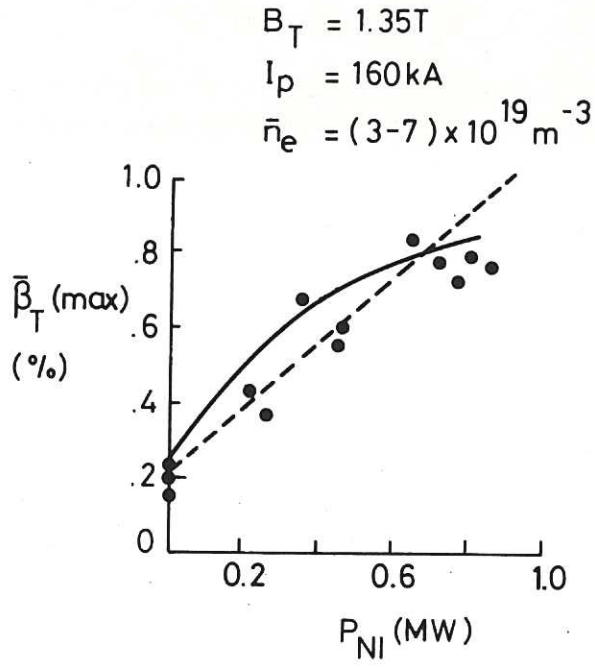

Fig.14 Variation of $\bar{\beta}_T$(max) with injection power for a series of discharges similar to Fig.7. The solid curve superimposed on the data follows equation (4.3).

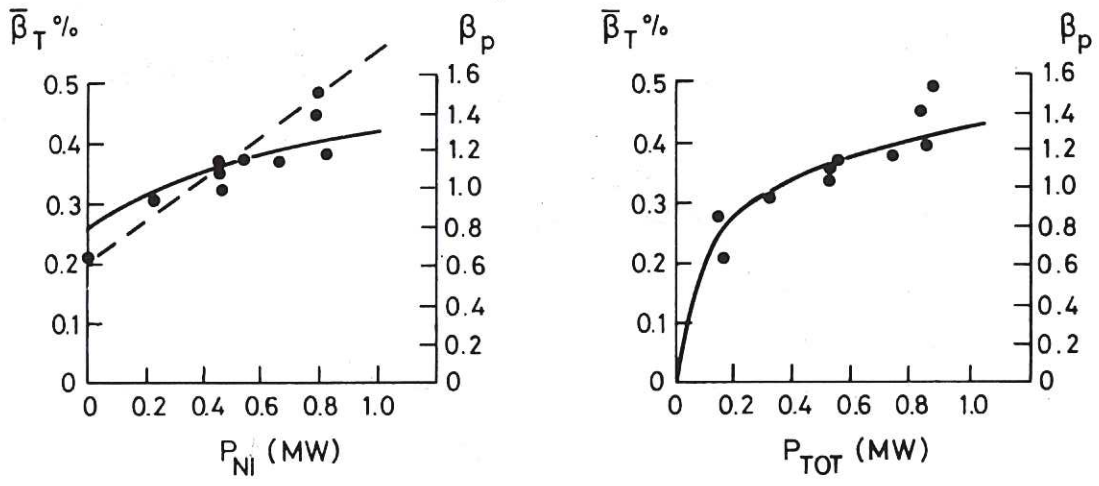

B_T = 1.35 Tesla

I_p = 100 - 110 kA

(a) $\bar{n}_e = (4-5) \times 10^{19}\ m^{-3}$ (b)

Fig.15 Variation of $\bar{\beta}_T$(max) with (a) injection power and (b) total power at constant density for B_T = 1·35 T, I_p = 100 kA. The solid curves superimposed on the data follow equation (4.3).

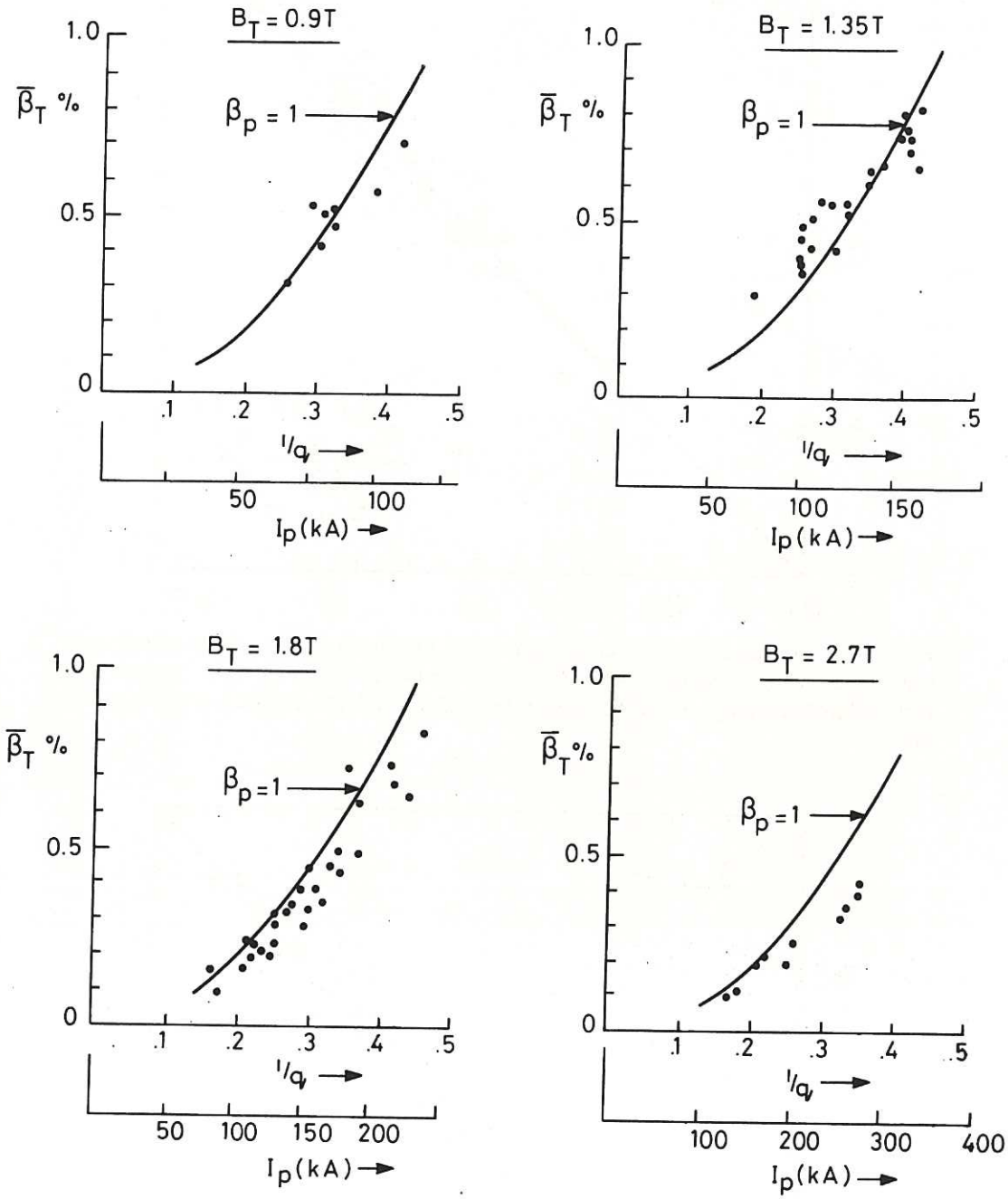

Fig.16 Variation of $\overline{\beta}_T$(max) with plasma current for four different magnetic fields B_T = 0·9, 1·35, 1·8 and 2·7 T. The curves represent β_p = 1·0.

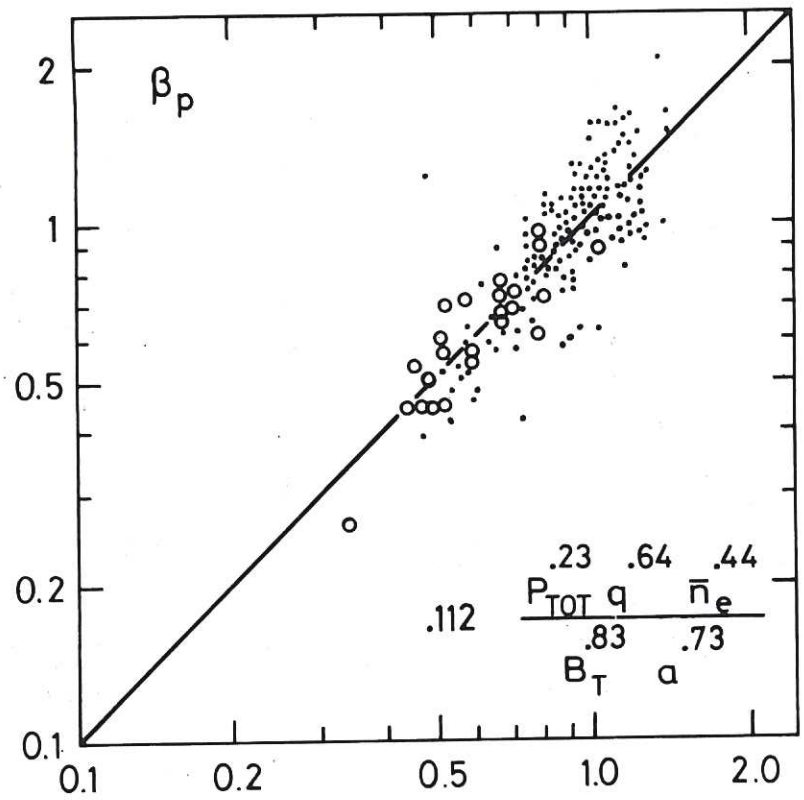

Fig.17 Plot of diamagnetic β_p versus values given by equation 4.2 for ohmic discharges (open circles) and discharges with neutral injection (solid circles) for both titanium and carbon limiter discharges in DITE. B_T is in Tesla, $\bar{n}_e$ in 10^{19} m^{-3}, a in metres and P_{TOT} in MW.

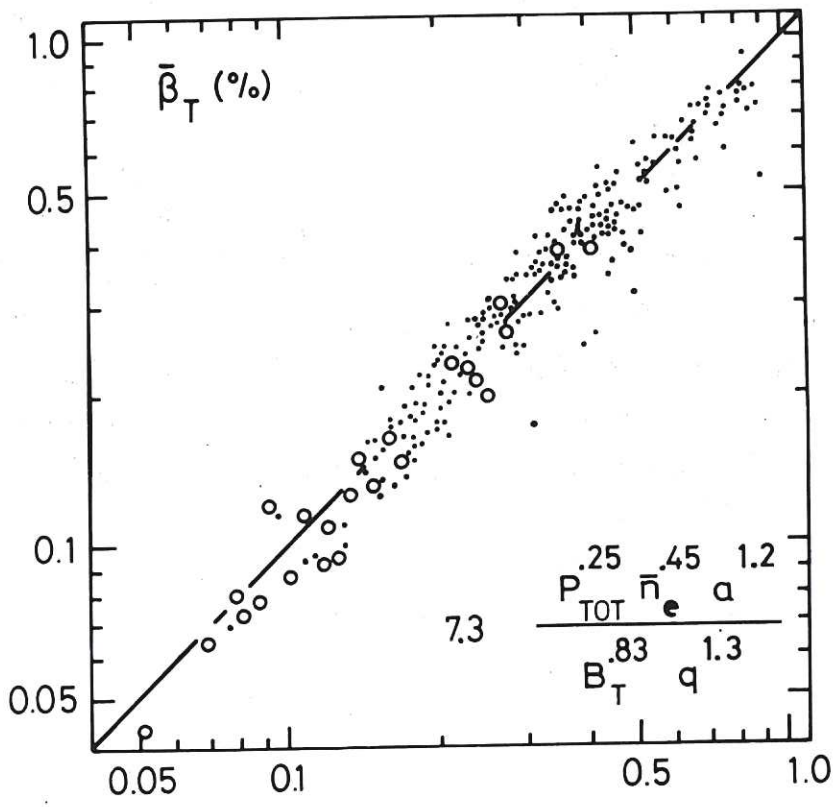

Fig.18 Plot of $\bar{\beta}_T$ estimated from diamagnetic loop against values given by equation 4.3. Symbols as Fig.17.

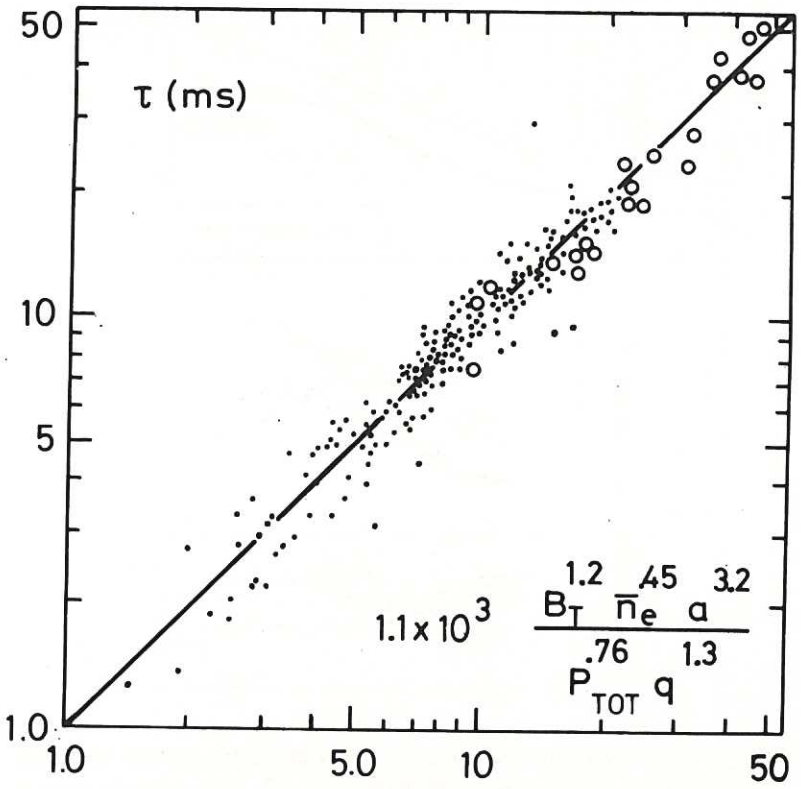

Fig.19 Plot of τ_E estimated from diamagnetic loop and the total power input against values given by equation 4.3. Symbols as Fig.17.

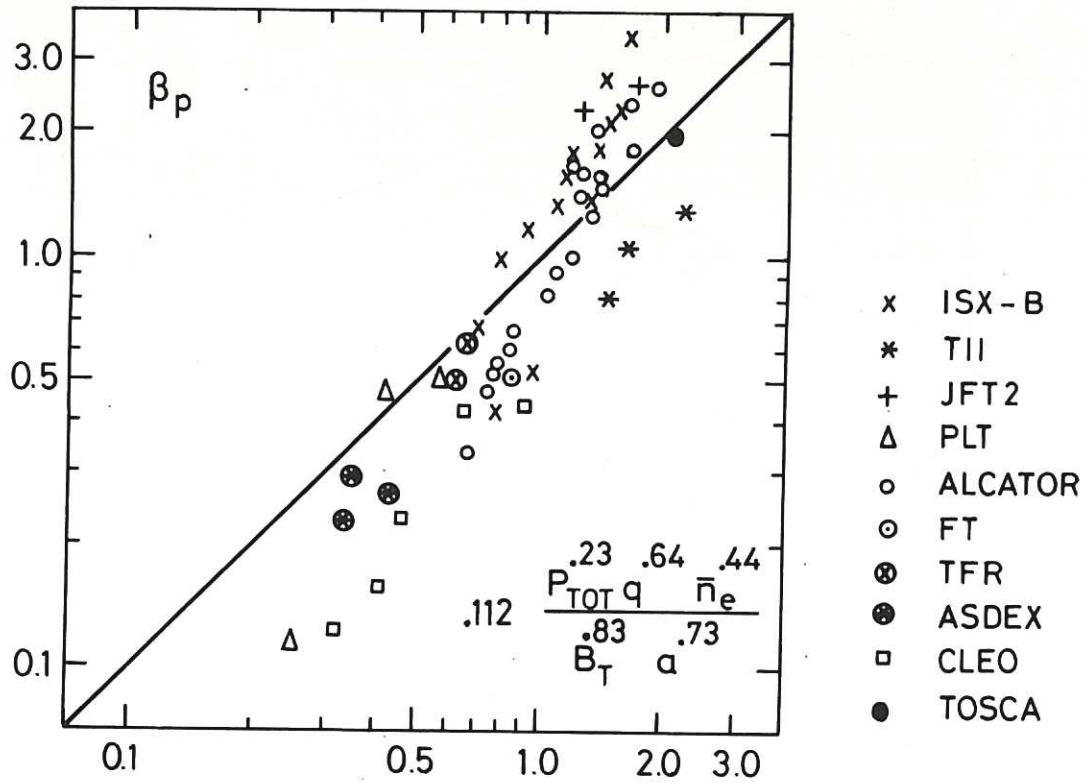

Fig.20 Plot of experimental estimates of β_p for other tokamaks against values given by equation 4.2.

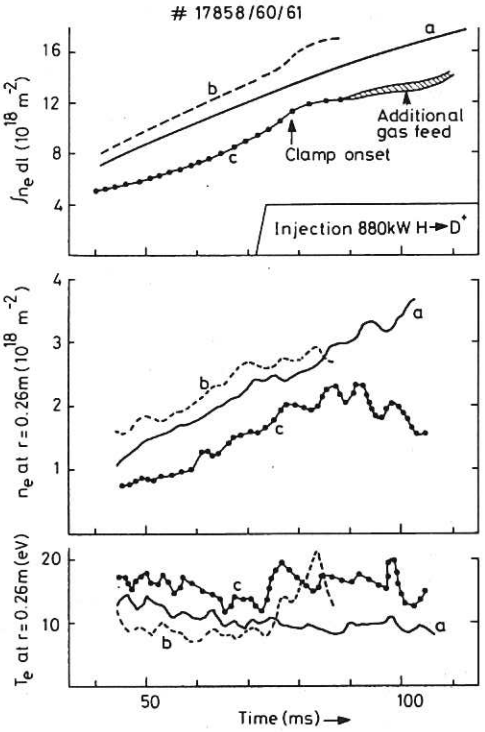

Fig.21 Time evolution of line average density, edge density and edge temperature. (a) is an ohmic discharge and (b) and (c) are discharges with neutral injection which exhibit the density clamp. B_T = 1·35 T, I_p = 100 kA.

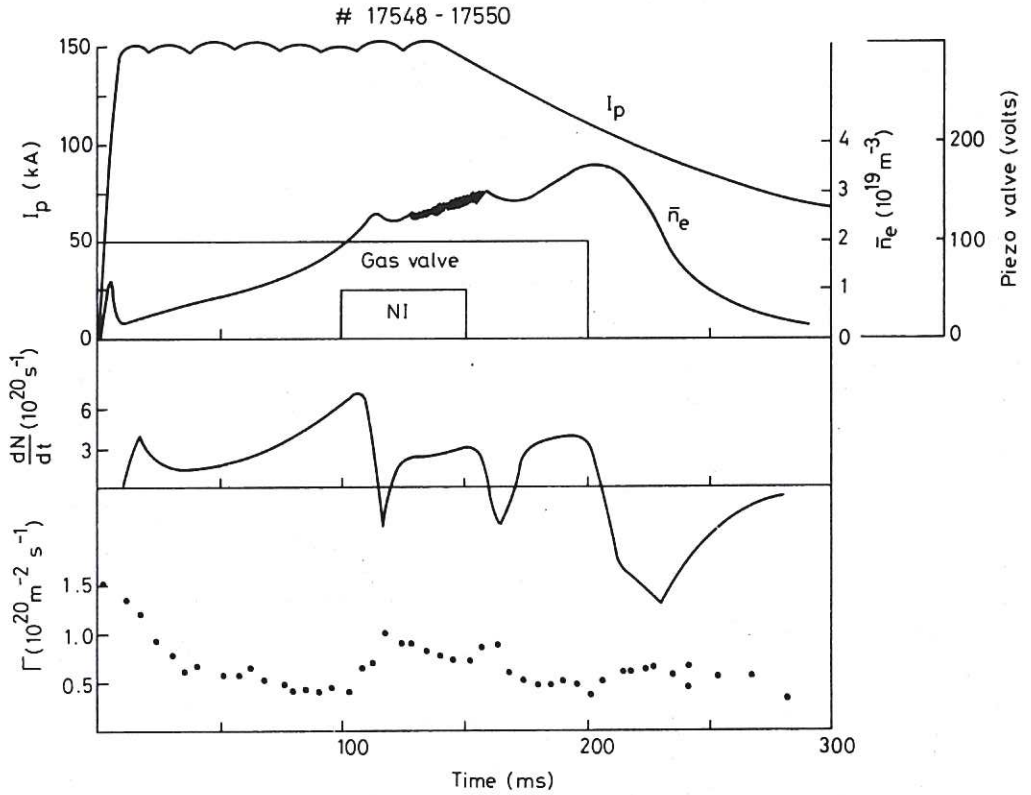

Fig.22 Time evolution of I_p, n_e, dN/dt and deuterium flux in the scrape-off layer, Γ, for a discharge which exhibits the density clamp on injection. B_T = 2·03 T, P_{NI} = 1 MW.

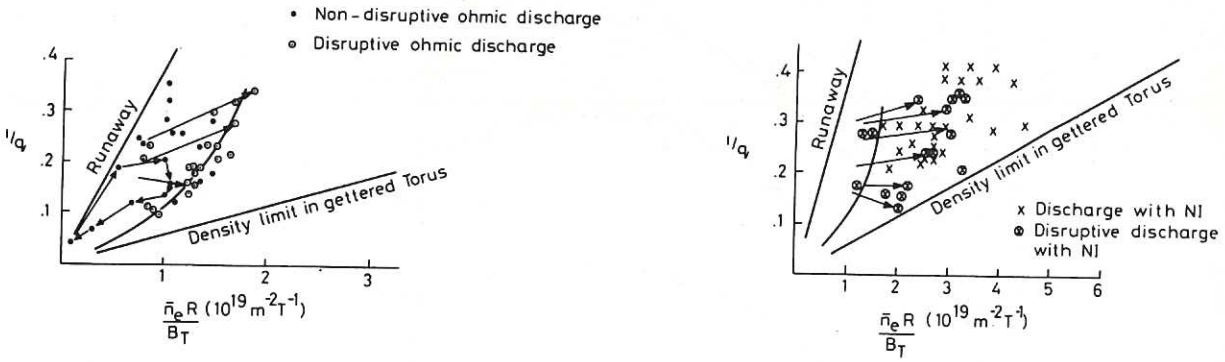

Fig.23 Operating diagram for ohmic discharges and with neutral injection both without titanium gettering. $B_T = 1{\cdot}35 - 2{\cdot}7$ T. $P_{NI} < 1$ MW.

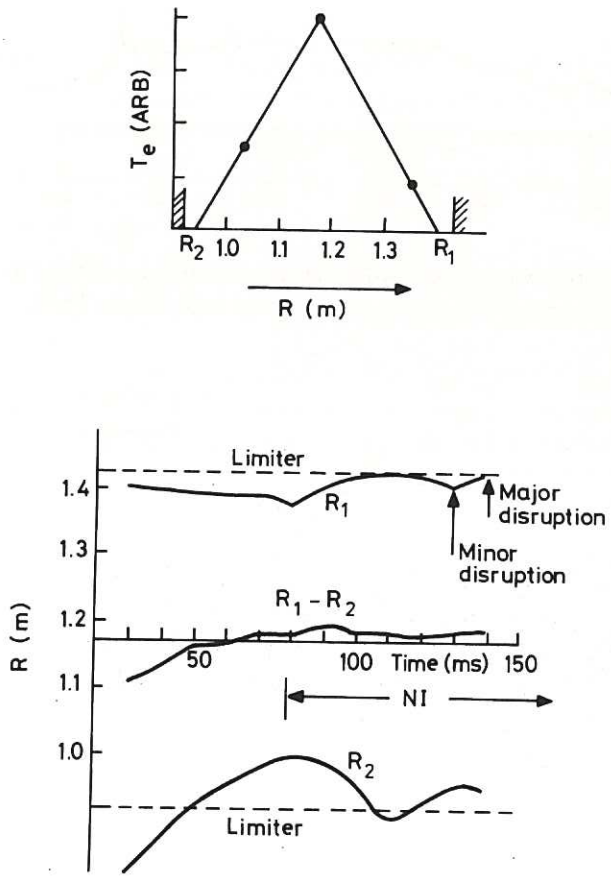

Fig.24 Temperature profile width as a function of time for a discharge with neutral injection but without gettering.

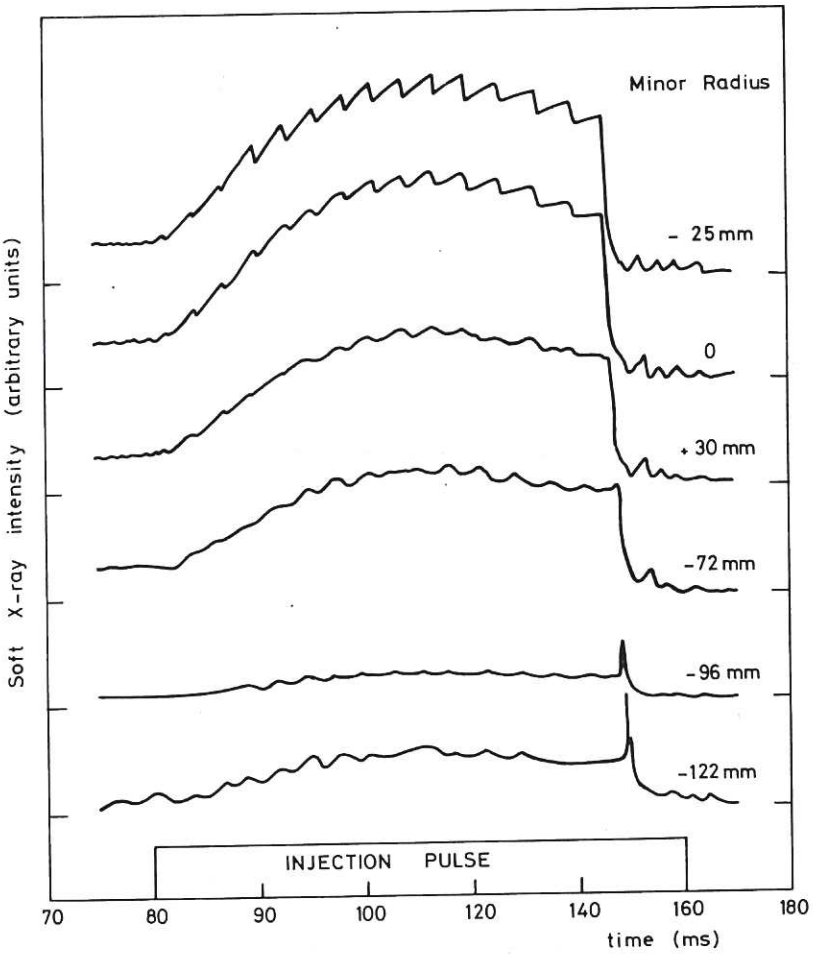

Fig.25 Behaviour of soft x-ray signals as a function of time for various chords. The discharge reaches the high density limit.

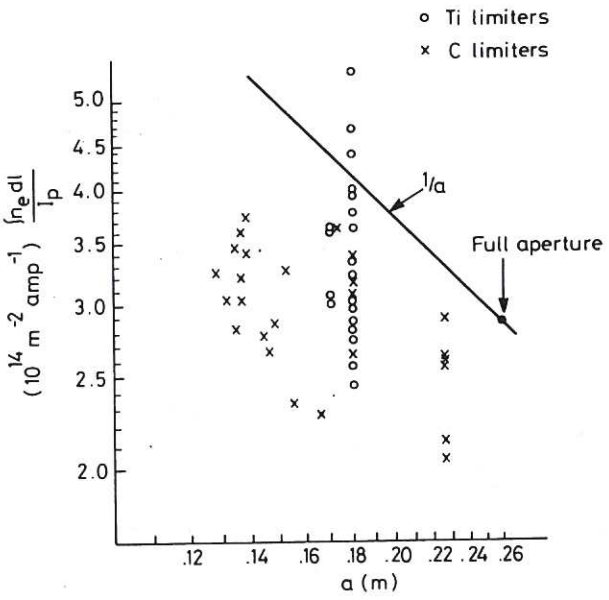

Fig.26 $\int n_e d\ell / I_p$ versus minor radius for discharges with either titanium or carbon limiters. $B_T = 1{\cdot}35 - 2{\cdot}7\,T$, $P_{NI} < 1\,MW$.

HER MAJESTY'S STATIONERY OFFICE

Government Bookshops

49 High Holborn, London WC1V 6HB
(London post orders: PO Box 276, London SW8 5DT)
13a Castle Street, Edinburgh EH2 3AR
Brazennose Street, Manchester M60 8AS
Southey House, Wine Street, Bristol BS1 2BQ
258 Broad Street, Birmingham B1 2HE
80 Chichester Street, Belfast BT1 4JY

Publications may also be ordered through any bookseller